



Crustal Structure and Ascent of Fluids and Melts Beneath Merapi: Insights From Geophysical Investigations

5

Birger G. Lühr, Ivan Koulakov,
and Wiwit Suryanto

Abstract

The magma plumbing system of Merapi volcano is a key for understanding its eruptive activity and thus has received scientific interest for a considerable time. First detailed attempts to resolve the volcano's internal structure and alleged magma reservoir were carried out at the beginning of the 1990s and included measurements of electrical conductivity, material density, seismic velocities as well as geodetic parameters and surface deformations. Major questions addressed were: (1) where do the fluids and magmas come from; (2) what are the magma ascent paths; (3) where are fluids and partial melts stored; and (4) what is the size and geometry of the magma and fluid reservoirs and the volcanic conduit? Here we review experi-

ments and findings we made during various stages of investigation at Merapi volcano, and also discuss selected projects by other teams and projects. By using seismic methods different crustal zones could be identified with low-velocity values and high V_p/V_s ratios, which can be explained as fluid- and melt-hosting zones. Large-scale joint seismic experiments (MERAPI, MERAMEX and DOMERAPI) displayed seismic attenuation and scattering effects seen in the shallow portion of the edifice, revealed the presence of fluid percolation and subvertical fluid-magma transfer zones, and identified crustal and near-Moho magma reservoirs that are being off-centred to the north. The complementary results of these projects contributed to a new structural image and understanding of the deep structure of Merapi over a depth range of more than 100 km. These results are valid not only for Merapi but now serve as an important example of the crustal structure considered for subduction volcanoes elsewhere.

B. G. Lühr (✉)
Helmholtz-Zentrum Potsdam, Deutsches
GeoForschungsZentrum GFZ, Telegrafenberg,
14473 Potsdam, Germany
e-mail: ase@gfz-potsdam.de

I. Koulakov
Institute of Petroleum Geology and Geophysics,
SB RAS, Prospekt Akademika Koptyuga 3,
Novosibirsk 630090, Russia

W. Suryanto
Geoscience Research Group, Department of Physics,
Universitas Gadjah Mada, Sekip Utara Bulaksumur,
Yogyakarta 55281, Indonesia

Keywords

Crustal structure • Subduction zone • Merapi
magma plumbing system • Geophysical
investigations • Seismic tomography

5.1 Introduction

To understand a volcanic system like Merapi, unravelling the internal structures at crustal and mantle depths is important. However, investigating the internal geophysical and geochemical structure of an active stratovolcano with a sufficiently high resolution is challenging because of its heterogeneous construction. The alternation of lava beds, block-and-ash-flow layers, surge and lahar deposits as well as igneous intrusions, all overprinted by erosion, leads to a heterogeneous mixture of materials with contrasting physical properties, which makes them challenging for many geophysical investigations. Seismological investigations significantly contributed to the understanding of the internal and physical structure of the Merapi edifice (Ratdomopurbo 1995; Ratdomopurbo and Poupinet 1995). Specifically, the localisation of seismic events and the first classification of different seismic signals that could be distinguished from each other led to the detection of a zone with very low seismicity and anomalously high attenuation of seismic waves at depths of 1–2 km below the summit. This zone was interpreted as a shallow magma reservoir within the edifice, while the main magma reservoir was supposed to start at 4–5 km depth, where the volcanic seismicity fades out again (Ratdomopurbo 1995; Ratdomopurbo and Poupinet 1995). In this chapter, we provide an overview of selected major projects with a contribution from German institutions, highlighting a decade-long Indonesian-German collaboration, student graduation and exchange. These projects are also considered in context with other collaborators, laboratories, partners, and projects from several other countries.

One of the first systematic structural investigations of the Merapi cone were carried out during the Indonesian-German MERAPI project (Mechanism Evaluation, Risk Assessment, and Prediction Improvement) in the years 1997–2002 (Zschau et al. 2003) and complementing research activities of scientists from France, Japan, and the USA. In the framework of the MERAPI project, comprehensive geophysical structure

investigations were carried out to determine: (1) the density structure and mass distribution using gravity measurements; (2) volume changes based on tilt and GPS measurements; (3) the electrical conductivity structure using magnetotelluric (MT), long offset time-domain electromagnetic (LOTEM) and geoelectrical measurements; and (4) the seismic structure of Merapi using active and passive seismological experiments.

During the MERAPI project and later until 2004, efforts to resolve the crustal structure beneath Merapi were able to determine details of the physical parameters and information about the complex geological architecture of the volcano. Nevertheless, important questions related to the volcanic system with its supposed magma reservoir, the ascent path of fluids and partial melts, and the way Merapi is embedded in the subduction process remained poorly constrained. The finding that Merapi as a volcano at a subduction zone—the Sunda Arc—is fed through a complex ‘plumbing’ system, which involves not only shallow structures beneath the volcanic edifice but also deep structures and processes within the underlying crust and upper mantle, led to the design of the larger seismic experiment MERAMEX (MERapi AMphibious EXperiment) (Bohm et al. 2005). Essential scientific and logistical support, and an important student and scientific exchange programme, was realised together with the Volcanological Survey of Indonesia (VSI) in Bandung, the Volcanological Technology Research Centre (BPPTK) in Yogyakarta, the Gadjah Mada University (UGM) in Yogyakarta, the Institut Teknologi Bandung (ITB) and the Indonesian Meteorology, Climatology and Geophysical Agency (BMKG) in Jakarta.

During the MERAMEX project period from 2004 to 2007, we could image strong seismic velocity anomalies and interpret the fluid and magma ascent paths and storage regions down to >100 km depths. However, the final 10 kms to the surface could not be resolved in detail. This shallower portion was investigated in detail by the interdisciplinary DOMERAPI project (Budi-

Santoso and Lesage 2016; Byrdina et al. 2017; Widiyantoro et al. 2018). DOMERAPI commenced in 2013 as a four-year-long international scientific research project led by French scientists at the Institut de Physique du Globe de Paris (IPGP), with support from the Institut des Sciences de la Terre (ISTerre) at the Université Grenoble Alpes and in partnership with the Laboratoire Magmas et Volcans (LMV) at the Université Clermont-Auvergne, the Institut des Sciences de la Terre d'Orléans (ISTO), the Indonesian Center for Volcanology and Geological Hazard Mitigation (CVGHM), Badan Geologi (VSI), the Institut Teknologi Bandung (ITB), GFZ Potsdam (Germany) and the United States Geological Survey (USA). In the framework of DOMERAPI, a dense network of seismographs was installed from October 2013 to mid-April 2015, the collected data of which were combined with data from the permanent seismic network of BMKG.

While the data analysis of these three major projects (MERAPI, MERAMEX, DOMERAPI) continues, the results have already led to an advanced and fundamentally more comprehensive understanding of Merapi as a volcano-magma system within the Sunda arc subduction system. In the following sections, the different geophysical efforts from the outlined research projects and their key scientific achievements are described in further detail.

5.2 GPS, Tilt and Gravity Measurements

Volcano geodesy includes the basic techniques and key parameters of volcano activity monitoring, providing information about its status, structure and dynamical processes (e.g., Dzurisin 2007). Some twenty years ago, Indonesian researchers in cooperation with scientists from France, Japan and the United States focused deformation experiments mainly on the summit area of Merapi, recognising mass and volume changes related to the dynamic behaviour of the Merapi lava dome. Various methods and techniques were tested and applied, including:

- (1) visual observations of the dome with a telescope camera located at an observation post in 12 km distance (Purbawinata et al. 1996);
- (2) remote sensing techniques such as stereophotogrammetry using a kite (Kelfoun 1999);
- (3) electronic distance measurements on a trilateration network (Young et al. 2000);
- (4) first attempts with InSAR technology using corner reflectors and campaign GPS surveys (Nandaka 1999); and
- (5) the operation of uniaxial horizontal platform tiltmeters (Subandriyo et al. 1997). At two flank sites uniaxial horizontal platform tiltmeters were installed; one location with a single instrument and the other with 5 instruments installed within an area of about 20×30 m (Beauducel and Cornet 1999).

Within the MERAPI project several flank sites were chosen for permanent multiparameter stations equipped with GPS receivers, tiltmeters and seismometers to observe edifice changes related to dynamic internal processes. Seismic studies by Ratdomopurbo and Poupinet (1995) suggested that a small shallow magma reservoir is indicated by an aseismic zone within the edifice. The multiparameter stations were installed at altitudes of 1280–2020 m as a ring-profile-constellation in respect to Merapi, aiming to capture the largest flank deformation rates at these sites. Another aim was to observe displacements caused by inflation or deflation with continuous precise vertical tilt measurements by applying a new array technique with borehole tiltmeters in combination with a Differential Global Positioning System (DGPS) (Rebscher et al. 2000a). A variety of further sensors were added as supplements and, therefore, the stations were acting as multi-parameter stations. Horizontal and vertical displacements were observed by using four permanent deformation measurement sites at the flanks of Merapi. A fifth receiver served as a reference station located at BPPTK in Yogyakarta (100 m asl). This local differential GPS network was tethered in the regional GEODYS-SEA net (Wilson et al. 1998) via the GPS-point Butuh at 30 km distance to Merapi's summit and 27 km to Yogyakarta.

Tilt measurements were conducted at the four flank stations with arrays of three shallow biaxial

borehole tiltmeters (Applied Geomechanics TM722A and TM722B). The instruments of an array at each site had a nominal resolution of 0.1 μrad and 1.0 μrad , respectively, installed in boreholes at 3–4 m depths and distances of 50–90 m (Westerhaus et al. 1998; Rebscher et al. 2000a). The array technique provided the possibility to distinguish between local and regional tilt signals, and the installation in boreholes allowed the reduction of near-surface disturbances and biaxial quasi-continuous measurements with sampling intervals of 5 min, allowing adequate time resolution. This effort was required to recognise the relatively small volcanic tilt changes on the flanks compared to those obtained at the summit of Merapi. Unfortunately, soon after the project ended, the stations stopped functioning due to vandalism, theft and a lack of maintenance.

Because meteorological and hydrological records were required for the correct interpretation of the high precision deformation data, a variety of auxiliary sensors were installed to record local environmental parameters. These allowed the detection and correction of local disturbances in the recorded data (Westerhaus et al. 1998; Rebscher et al. 2000a), and provided meteorological data required for the interpretation of other measured parameters such as seismicity, electrical conductivity, chemistry and temperature of fumarole gases and hydrology.

Surprisingly, the GPS and tilt data collected on the mid and lower flanks of Merapi did not record any significant changes in horizontal or vertical axis or displacements (Rebscher et al. 2000b). During the volcanic crisis in January 1997 (eruptions on 14 and 17 January) and July 1998 (eruptions on 11 and 19 July) only minor tilt anomalies could be identified, with a tilt signal of maximum 1 μrad associated with the 14 January 1997 explosive event (Westerhaus et al. 1998). The loading of pyroclastic flows in 1998 produced a static tilt anomaly of $\sim 8 \mu\text{rad}$ in all tiltmeters. The lack of relatively large flank deformations associated with the volcanic activity did not support the existence of a large shallow magma reservoir inside the Merapi edifice. Accordingly, later related projects and

monitoring approaches concentrated on the notably deforming summit region (e.g., Budi-Santoso et al. 2023, Chap. 13).

In the summer of 1997, a gravity repetition network was established around Merapi (Gerstenecker et al. 1998a). The network consisted of 23 stations forming three loops around Merapi at different altitudes. The first loop connected altitudes of 100–500 m asl and the second one connected all stations at medium altitudes (1000–2000 m asl). The third loop was located at the crater rim at 2900–2970 m. All three loops were connected to each other along a gravity profile at the north flank of Merapi (Gerstenecker et al. 1998a). Gravity observations were carried out alongside GPS measurements, using geodetic 2-frequency receivers (Trimble 4000 SSE/SSI and Leica C322/RS299) to determine vertical crustal movements at the stations that influence secular gravity changes directly via the free air- or Bouguer-gradient. Gravity changes due to vertical crustal movement were eliminated for the estimation of the gravitational effect of mass movements in and outside of the volcano (Gerstenecker et al. 1998a). In each measurement campaign, four LaCoste&Romberg spring gravity metres were used. The calibration functions of the instruments and their changes in time were $\pm 5 \times 10^{-5}$. A change of the scale factor of 5×10^{-5} generates a virtual gravity change of about $38 \times 10^{-8} \text{ m/sec}^2$ (Gerstenecker et al. 1998a). The largest gravity difference amounted to $\sim 751 \times 10^{-5} \text{ m/s}^2$. Gravity differences at the installed network were observed four times at Merapi. Due to all limitations, the mean standard deviations of vertical crustal movements were $\pm 50 \text{ mm}$ (Gerstenecker et al. 1998a). The measured gravity and vertical crustal changes were, however, much smaller than expected before observed volcanic activity. Only near the crater rim, at altitudes of 2000–2970 m asl, a significant gravity increase (up to $100 \times 10^{-8} \text{ m/s}^2$) was detected and found to be associated with significant crustal subsidence in a range of up to -180 mm (Gerstenecker et al. 1998a). Gravity changes around the summit of Merapi increased during the campaign by $\sim 80 \times 10^{-8} \text{ m/s}^2$ (80 μgal), which may have been caused

by mass movements in- and outside of the volcano. Especially the changing topography of the dome in the immediate neighbourhood of the summit stations was thought to be responsible for these changes, further supported by observations from synthetic aperture radar (SAR) and photogrammetric images (Gerstenecker et al. 1998b). Gravity data inversion gave a mean density of 2241 kg/m^3 and an estimated porosity range of 10–20% (Tiede et al. 2005). Based on this mean density, Tiede et al. (2005) derived a subsurface 3-D density model of the Merapi and Merbabu region by the analysis of 443 campaign gravity points. Using a least-squares inversion approach, maximal density anomalies between -242 kg/m^3 and $+264 \text{ kg/m}^3$ were found relative to the mean density (Fig. 5.1), confirming relatively high rock porosities in the Merapi region (Tiede et al. 2005).

5.3 Electrical Resistivity Structure

The resistivity structure of Merapi was investigated using different electromagnetic methods. Applied methods, such as direct current electrical resistivity tomography (DC) and magnetotellurics (MT), were used to determine the spatial distribution of the electrical conductivity from natural geomagnetic and geoelectric field variations. Of these, the DC method has the highest spatial resolution but the smallest penetration depth, while MT has the largest penetration. The long-offset transient electromagnetic (LOTEM) method fills the gap between DC and MT (Telford et al. 1990).

The DC survey comprised two different approaches (Friedel et al. 1998), where benchmarks of resistivity were derived for pyroclastic material varying in saturation with air, meteoric water and solfataric water. These measurements

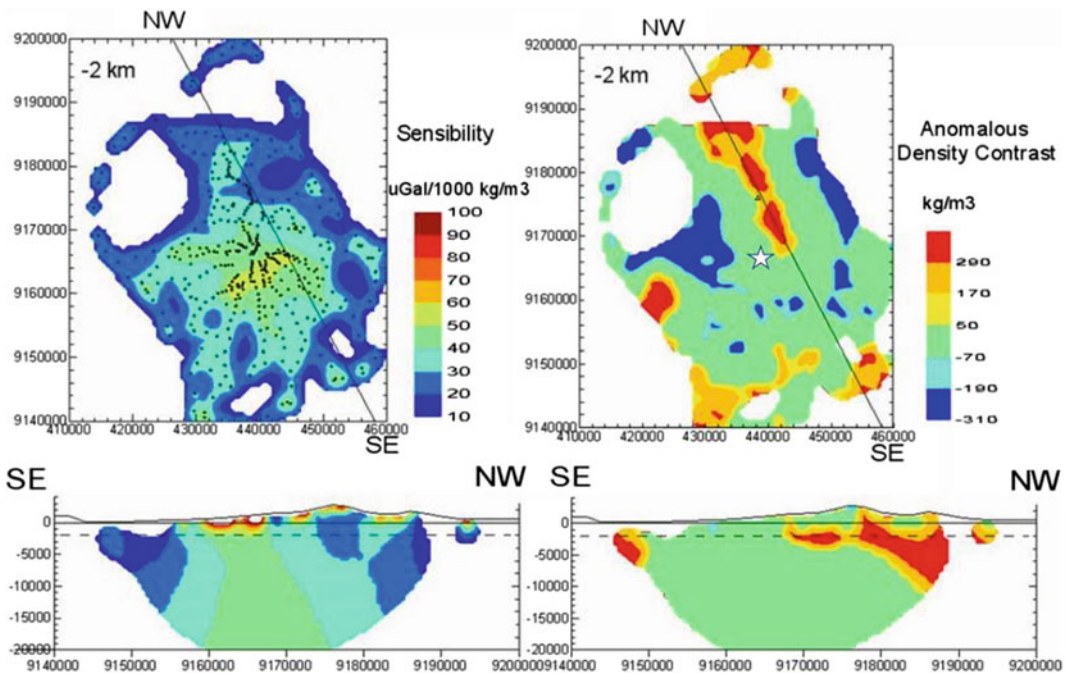


Fig. 5.1 Horizontal and vertical cross-sections of the 3-D anomalous density model (right) and gravity sensitivity distribution of the model (left). The vertical SE-NW profiles follow the 152°N course of an intrusive body. The sensitivity pattern corresponds to the station distribution

and the relative size and position of 20,000 cells. Maps are in UTM coordinates (after Tiede et al. 2005). The summit area of Merapi is marked on the right map by a white star and gravity measuring points are marked by black dots

were taken in quasi-homogeneous conditions at selected flank locations and at the Woro fumarole field near the summit, which was later destroyed by the 2006 and 2010 eruptions. LOTEM, which measures voltage decay curves with electric and magnetic receivers after a polarity reversion of a current (DC) in an electric dipole transmitter at several kilometres distance (Strack 1992), was used to resolve the structure of Merapi down to a depth of 800–1000 m below the surface by recording LOTEM data at 41 receiver locations on a 10 km W-E profile and a 15 km S-E profile. Signals were transmitted from a transmitter on the northern flank in SELO, two transmitters on the western flank (AGLI, BABA) and one transmitter on the southern flank (KINA) (Müller et al. 2002). Three dipole–dipole profiles with lengths of 2.3 km, 2.6 km and 3.6 km and dipole widths of 200 m were conducted along the west, north and south flanks, respectively (Müller et al. 2002).

Large scale MT measurements, which use natural time-varying electromagnetic fields that originated in the Earth's magnetosphere (Vozoff 1991), were carried out along a profile crossing Central Java with the aim to determine geomagnetic induction vectors (Müller and Haak 2004), recognise good conductors and detect striking faults. MT recordings were made at a total of 65 sites in a period range of 0.001–1000 s. The measurements took place at two different scales: 20 sites were set up to obtain information about the regional electric conductivity distribution (10 of them at a 130 km profile) (Ritter et al. 1998), while 40 locations were selected in the vicinity (i.e. within a 15 km radius) of Merapi. The best data quality was obtained at a site 50 km north of Java on an uninhabited island of the Karimunjawa archipelago.

At Merapi, the general resistivity structure was derived from LOTEM 1-D inversion and 3-D modelling (Müller et al. 1998; Müller 2000; Commer et al. 2005, 2006), DC 2-D inversion (Friedel et al. 1998, 2000; Byrdina et al. 2017) and MT 1-D inversion and the 3-D modelling (Müller 2004). For the northern part, a four-layer model could fit the data while for the southern

part a six-layer model best fitted the measured data curve (Fig. 5.2).

The main features of the combined model are as follows: on the western and southern flank, the soundings show electrical resistivities $>10,000 \Omega\text{m}$ within the first 200–300 m beneath the surface, which drop rapidly to values $<100 \Omega\text{m}$ and $10 \Omega\text{m}$, respectively, to a resolved depth of 800 m. DC results show that the top layer decreases in resistivity down the flanks of Merapi. The resistive layer is underlain by a conductive layer with resistivities of $10\text{--}30 \Omega\text{m}$. The conductor was identified by all three methods, and geometrically follows the topography of the volcano, as derived from induction vectors of the MT measurements (Müller 2004) and by the LOTEM data (Müller 2000). Further, a conductive feature was found 9 km south of the summit. A reanalysis of the LOTEM data (Kalscheuer et al. 2007) depicted again a layering that follows the topography of Merapi. At a depth range of 500–1000 m, the resistivity of the outward dipping layers decreases rapidly downwards into a good conductor with resistivities $<10 \Omega\text{m}$. For the deepest layer, the authors determined a resistivity of $0.4 \Omega\text{m}$, which is quantitatively explained with a combination of ion and electron conductivity caused by saline fluids and hydrothermally altered minerals. Furthermore, the final model supports a hypothesis from the interpretation of central-loop transient electromagnetic (TEM) data of an E-W oriented fault structure below Merapi's southern flank, ~ 7.3 km south of the summit. To the north of this structure, the top of this conductor is located at a shallow depth of 500–1000 m. Kalscheuer et al. (2007) hypothesised that this fault structure coincides with an ancient avalanche caldera rim or, alternatively, may be a structure generated on the slope by gravitational spreading caused by a flow of flank material on weak substrata due to volcanic loading (Delcamp et al. 2008).

Friedel et al. (2000) suggested that the increase of conductivity above values of 20 mS/m might indicate the contact zone of a hydrothermal system beneath the summit, rather than freshwater saturation of porous pyroclastic deposits. In the framework of the more recent

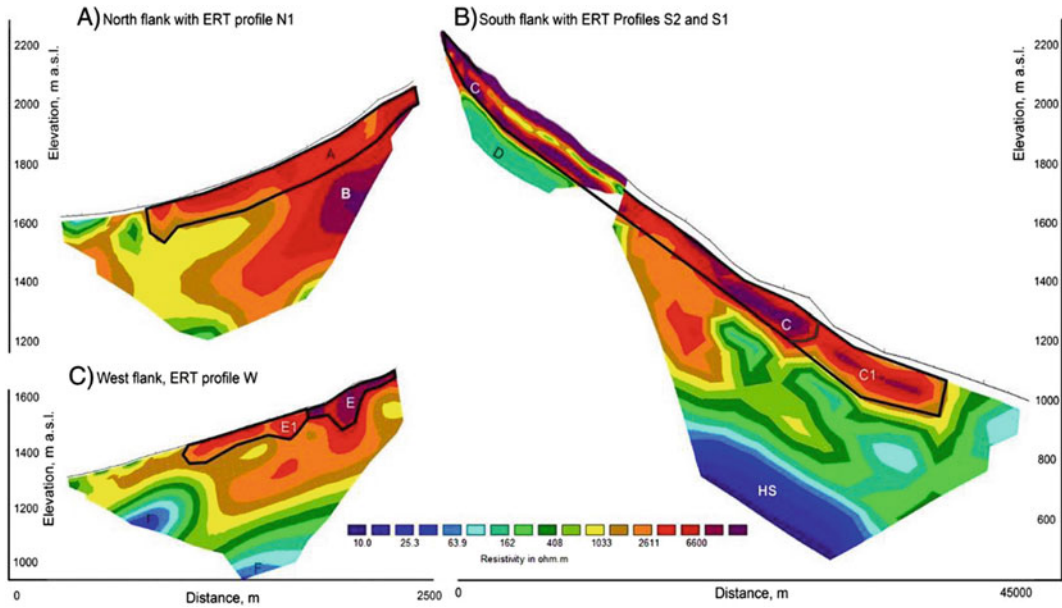


Fig. 5.2 Comparison of the resistivity structure at north and south flanks. Vertical elevation scale is common for north (A) and south (B) flanks. Conductive structures ‘HS’ with resistivity $< 10 \Omega\text{m}$ and ‘F’ with resistivities of $40\text{--}80 \Omega\text{m}$, probably representing a hydrothermal altered fluid-saturated layer or a hydrothermal system below the west and south

flank at a depth of 1000 m. At the surface, recent andesite lava flows below the south flank (unit ‘C’) are characterised by extremely high resistivities exceeding $100,000 \Omega\text{m}$. Units ‘A’, ‘C1’ and ‘E’ with resistivities of $1500\text{--}5000 \Omega\text{m}$ represent pyroclastic flow deposits of Old Merapi as well as lahar and airfall deposits (Byrdina et al. 2017)

DOMERAPI project, Byrdina et al. (2017) investigated the hydrothermal system of Merapi using electrical resistivity tomography (ERT), self-potential measurements and CO_2 flux mapping. Distinct low-resistivity bodies were interpreted as part of an interconnected hydrothermal system at the base of the south flank and in the summit area (Byrdina et al. 2017). In the summit area, a sharp resistivity contrast at the ancient crater rim of Pasarbubar separated a conductive hydrothermal system ($20\text{--}50 \Omega\text{m}$) from the resistive andesite lava flows and pyroclastic deposits ($2000\text{--}50,000 \Omega\text{m}$). The existence of preferential fluid circulation along this ancient crater rim was also indicated by self-potential data. In the vicinity of the active crater rim and close to the ancient crater rim of Pasarbubar, diffuse CO_2 degassing was observed with a median value of $400 \text{g/m}^2\text{d}$. The total CO_2 degassing mass rate across the accessible summit area with a surface of $140,000 \text{m}^2$ was around 20t/d , which equals to $\sim 10\%$ of the volume of

CO_2 estimated to have degassed before the 2010 eruption (Toutain et al. 2009).

On the southern flank of Merapi, the resistivity model shows a pronounced stratification. While recent andesite lava flows are characterised at the surface by resistivity values $>100,000 \Omega\text{m}$, resistivity values as low as $10 \Omega\text{m}$ have been encountered at a depth of 200 m at the base of the south flank, interpreted as reflecting the presence of the hydrothermal system (Byrdina et al. 2017). However, no hints for such a hydrothermal system were found on Merapi’s northern flank, which might be caused by the asymmetry of the heat supplying source of Merapi, whose activity is moving south, and/or by the asymmetry in topography caused by the presence of Merbabu volcano to the north. Thus, Byrdina et al. (2017) suggested that lithological layers on the south flank of Merapi separate the hydrothermal fluids with gaseous fluids rising through the crater rims, while liquids flow downwards to the base of the edifice.

At greater depth of ~ 1.5 km bsl, very low resistivity values of $<1\text{--}3 \Omega\text{m}$ were detected through MT data, extending as far as 15 km from the summit of Merapi. Results from a first regional campaign in 1997 (Hoffmann-Rothe et al. 1998; Ritter et al. 1998) showed that such low values can be found in the crust beneath Central Java but that partial melts are not likely to explain the conductive layers at Merapi at depths of ~ 1 km. The moderately conductive layer ($10\text{--}30 \Omega\text{m}$) covers a region of several 10 km^3 , while the high conductivity bottom layer ($<1\text{--}3 \Omega\text{m}$) could also be identified by MT measurements outside the area covered by Merapi down to 1800 m bsl (Ritter et al. 1998). Lloyd et al. (2007) investigated the hydrogeological situation in Central Java and described the presence of at least two aquifers, with the lower one often confined and saline. Commer et al. (2006) estimated a salinity range for the pore filling by applying conductivity measurements of NaCl solutions as a function of temperature and concentration (Keller 1988). For their model layers 1 and 2 (Commer et al. 2006), the maximal salinities of 0.2 and 0.7 eq. wt.% indicate a rather dilute solution. A low degree of salinity agrees with isotopic investigations at the summit of Merapi, showing that fumarolic water is mainly of meteoric origin, with only a small contribution of magmatic water (Zimmer et al. 2000). The deeper layers 3 and 4 (Commer et al. 2006) show increased salinities, and, while the salinity of seawater with a value of around 3.5 eq. wt.% falls well within the range of layer 3, the estimates for the bottom layer show a much higher concentration. Van Bemmelen (1949) pointed out earlier that the young Quaternary volcanoes of East Java are built upon a basement of plastic and not yet fully consolidated marine sediments. For weakly cemented marine rocks, usually Tertiary in age, the electrical conductivity can be very high because of a combination of ion and electron conductivity in claystones and micaceous clay. In this case, the low basement resistivities may well be explained by the intrusion of seawater beneath Java.

5.4 Active Seismic Measurements Explain Complex Earthquake Signals of a Stratovolcano

The influence of topography, the heterogeneous medium for propagating seismic waves and almost unknown source mechanisms lead to manifold difficulties in analysing and interpreting volcano-seismic signals. For locating and analysing natural seismic events within and beneath the edifice of Merapi—particularly for the separation of source, path and site effects—the seismic structure information is indispensable. Therefore, seismic profiles (Fig. 5.3) were already recorded through up to 30 three-component seismometers aligned radially to the volcano summit using a receiver spacing of 100 m in the framework of the MERAPI project in the late 1990s. Nearly 5 km away from the summit, in a radial fashion and at an altitude of about 1000 m asl, water basins were installed at three locations, and each filled with 40 m^3 water. In these basins, a 2.5 l mud gun was fired by an air pressure of 80–100 bar to generate well defined seismic source signals with high repeatability necessary to increase the signal energy by stacking up to 100 single shots and to improve the signal–noise ratio (Wegler et al. 1999).

Surprisingly, the recorded seismograms were characterised by unusually complicated wave fields that were difficult to explain by common standard seismic methods. Records near the source location showed a short and pulse-shaped waveform, while at greater distances, the signals spread out to longer wave trains. Only the p-phases showed, in traces, clear coherency, whereas later phases were mostly shear wave energy incoherent along the profile. Some of the coherent onsets were recognised with negative apparent velocities. They could be interpreted as refracted waves reflected at steeply dipping reflectors, while others may be backscattered surface waves, with some out of the profile lines (Luehr et al. 1998; Maercklin et al. 2000). Such complexity was later also identified at other volcanoes (Wegler 2003).

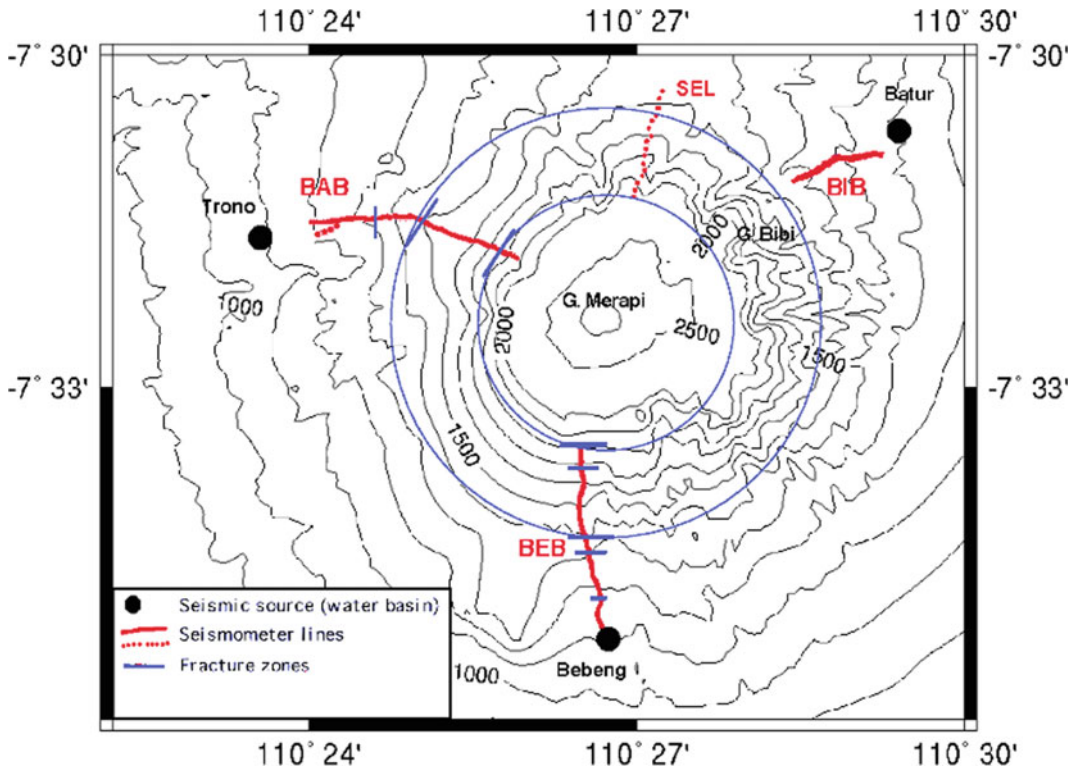


Fig. 5.3 Location of seismic lines measured in the frame of the MERAPI project in 1997, source points and mapped fracture zones. Profiles shown as dotted lines

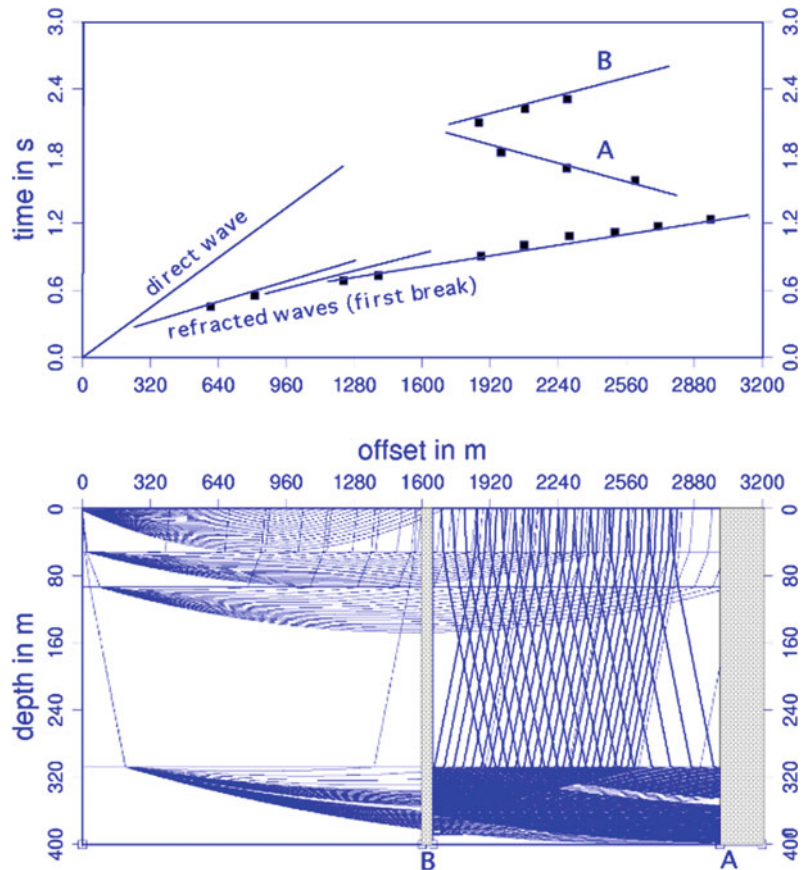
were not interpreted. Two circles mark the extent of possible weakness zones

Observed linear, coherent phases contained information on larger scale structures. To enhance these types of waves, all three spatial components were jointly processed using polarisation analysis (Maercklin et al. 2000). After processing, the first arrivals were recognisable up to 7.5 km distance, not far enough for penetrating the volcanic cone to the opposite side. Therefore, these records could not be applied for a travel time tomographic analysis. Direct S-waves were superimposed by the P-wave coda and only observable up to 1 km distance from the seismic source. 2-D ray-tracing supported the interpretation of first and later onsets. The resulting model is based on a layered 1-D depth profile of the P-wave velocity derived from first break travel times. The velocities range from some hundred m/s close to the surface to more than 3000 m/s at a maximum depth of ~ 300 m. As each model layer likely corresponded to

numerous different geological units, only an effective velocity was defined. With reflectors vertical to these layers, it was possible to fit the travel time curves of selected onsets. The model shown in Fig. 5.4 assumes a p- to s-wave conversion at reflector A, located ~ 3 km away from the source, to explain the lower apparent velocity of the reflected onsets A and B (Fig. 5.4).

The high impedance contrasts at both modelled reflectors were explained by structural heterogeneities (Maercklin et al. 2000). These fracture or weakness zones were mapped at Merapi using observed reflections on lines BEB and BAB (Fig. 5.3). The most prominent fracture zones on both profiles seem to be equidistant to the summit of Merapi and may belong to a larger, approximately circular zone of weakness with a diameter of ~ 4 km, which agrees well with the low resistivity zone found by electromagnetic

Fig. 5.4 Modelled ray paths and travel time curves for selected onsets of line BEB. The model is based on a simple 1-D velocity-depth function and reflectors perpendicular to the layers. Letters A and B denote reflectors and corresponding time curves; black boxes indicate measured travel times. The depth is defined in metres below the surface



measurements. White-coloured rocks and debris led to the speculation that the high-conductive anomaly detected at Merapi and the circular feature of low seismic velocity could be due to a hydrothermally altered zone surrounding the inner core or conduit of the volcano. Soil temperature and CO₂ gas flux measurements carried out at the summit from 2002 to 2007 (Toutain et al. 2009) support this idea. This study found degassing anomalies that appear to be controlled by structures identified as concentric historical crater rims (1768, 1872 and 1932), which may have undergone a hydrothermal self-sealing process that lowered permeability and porosity. Heap et al. (2019) showed that acid-sulphate alteration, common at Merapi and other volcanoes, can reduce the permeability at rock sample scale by up to four orders of magnitude as a result of pore- and micro-fracture filling mineral precipitation. Using these petrophysical data,

their calculations demonstrated that intense progressive alteration can reduce the equivalent permeability of a dome by two orders of magnitude, which is sufficient to increase pore pressure inside and beneath a dome such as that at Merapi.

A surprising observation in the recorded seismograms (Wegler and Luehr 2001a) was that the amplitude of the first onset decreases rapidly with increasing source-receiver distance, while the main part of seismic energy is included in the coda of the seismograms and shifted towards later travel times. The maximum energy of the coda waves moved with a group velocity of 200–400 m/s along the profiles. The coda waves were polarised horizontally but showed no preferred azimuths. This strange effect on the seismic signals can be explained physically by the inner structure of the volcanic cone, which is built up by alternating material of pyroclastic flow, lahar

and ash deposits. Big blocks and compact lava banks alternate with less intensively consolidated material. Layers vary in thickness and extension and were cut by erosion processes. These inhomogeneities with high acoustic impedance contrasts produce strong scattering effects which reduce the energy from the first onset so that it fades out after a distance of 7.5 km. For applying a travel time tomographic analysis, the first onset would have had to be detected up to 12 km distance. As this was not the case, the experiment was eventually discontinued.

Assuming that most of the energy in the seismograms was associated with multiple scattering and that S-waves dominated the coda, the observed waveform envelope was explained by the diffusion model (Dainty and Toksöz 1981). According to this model, the energy density as a function of time and space included the attenuation coefficients h_s and h_i as geophysical formation parameters. The parameter h_i described the energy loss of a seismic wave due to conversion to other forms of energy (e.g., heat) called intrinsic attenuation, while h_s denoted the energy loss due to scattering (Wegler et al. 2000; Wegler and Luehr 2001a, b). Interestingly, it was found that the resulting scattering attenuation was at least one order of magnitude larger than the intrinsic value. The frequency dependence of h_s was proportional to $f^{0.0}$, whereas h_i was proportional to $f^{1.6}$. At Merapi, the derived mean free path for generated airgun signals with an energy maximum of $\sim 7\text{--}8$ Hz was as low as $h_s^{-1} = 100$ m. This means that multiple scattering effects had to be considered for source-receiver distances greater than 100 m at Merapi, justifying the use of the diffusion model for source-receiver distances greater than several hundreds of metres. This result also explains the bad coherency of seismic traces with a chosen seismometer spacing of 100 m. No significant differences were found for the three different profiles in h_s . However, h_i of BAB on the west flank was 0.5 times smaller than h_i of BEB on the south flank and of BIB on the northeast flank, which might be correlated with the local geology (Wegler et al. 1999).

The natural seismicity of Merapi, particularly events located in the upper part of the volcano cone and called multiphase (MP) events, showed similar characteristics compared to airgun shot records. First onsets were weak and often difficult to recognise. The maximum energy of the wave trains was shifted by distance to later arrival times compared to small first onsets. Shear waves as body waves were nearly invisible.

5.5 Merapi's Magma Reservoir and Ascent Paths of Fluids and Partial Melts

After the first interpretation of the seismicity distribution, the main magma reservoir of Merapi was thought to be located at a depth of 4–5 km (Ratdomopurbo and Poupinet 1995), extending to a depth of 10 km or more because of the fade-out of the volcanic seismicity beneath 5 km below the summit. Later, the hypothesis of a main magma reservoir was supported by petrological data (Purbawinata et al. 1997). However, more recent petrological studies have shown that Merapi magmas are stored at multiple levels, ranging from the shallow conduit down to ~ 30 km (e.g. Chadwick et al. 2007, 2013; Costa et al. 2013; Preece et al. 2013; Deegan et al. 2016; Troll and Deegan 2023, Chap. 8).

Gossler (2000) analysed teleseismic event records at seismic monitoring stations located on the flanks of Merapi. Receiver functions (Yuan et al. 1997; Gossler et al. 1999) based on the analyses of P–S converted shear waves revealed structures in the crust, the Moho and the subsiding lithosphere plate. The application of the Receiver functions method allowed the properties and constitution of the deeper parts beneath Merapi down to the subducting slab to be inferred. However, the occurrence of strong multiple phases in the seismograms, interpreted as reverberations of the incoming waves between the down-going plate and the surface, impeded a detailed resolution of deeper structures. Moreover, a large magma reservoir could not be detected.

Besides, investigation of the polarisation of incident teleseismic waves showed an interesting effect depending on the analysed frequency band. Long-period waves above 10 s yield no significant differences between observed and theoretical calculated azimuths or incident angles, respectively, in which the incident angle represents a measure of the distance between a hypocentre of an earthquake and the receiver location. For higher frequencies with periods below 5 s, this changes dramatically. As a result of the polarisation analysis, the determined azimuths and incident angles of the incoming waves point towards the centre of Merapi, independent of the true location of an earthquake. This suggests that the hypocentres of the analysed earthquakes were located inside Merapi, a result interpreted as a topographic effect caused by the geometry of the cone-shaped volcanic edifice of Merapi (Gossler 2000).

Despite these geophysical studies, questions about the hypothesised magma reservoir, ascent paths of fluids and partial melts, and how Merapi is embedded in the subduction process, could not be answered. One reason for this was that all investigations were concentrated mainly on the edifice of Merapi, where, for instance, the small aperture of seismic stations in combination with the complex structure limited the retrieved information. The magma storage and complex feeding and plumbing system, which not only involves the shallow structures beneath the volcanic edifice but also deep structures and processes within the underlying crust and upper mantle, led to the design of the larger MERAMEX seismic experiment, which is further detailed below.

5.5.1 Deeper Structure Beneath Central Java

Regional-scale seismic tomography and the distribution of the Wadati-Benioff seismicity from the revised International Seismological Centre (ISC) bulletin constrains the subducting slab at the Sunda arc down to 1000 km depth (Lühr et al. 2013). A lack of robust data at shallow

depth can be compensated by using local earthquake data, which also provide more detailed information about the crustal structure and the volcanic plumbing system above the slab-related Wadati-Benioff zone beneath Central Java and Merapi. Results of the regional tomography suggest that the subducting slab cannot be represented by an oversimplified conveyor-type 2-D model. Considerable lateral and vertical variations in the slab thickness probably have effects upon the surface tectonics. In particular, the peculiar character of Merapi might be caused by a slab window that formed in the contact zone between two autonomously subducting oceanic plates (Koulakov et al. 2007).

Between May and October 2004, combined amphibious seismological investigations at 110°E were thus performed as part of the MERAMEX project (Reichert and Lühr 2005). A temporarily installed seismic network of 134 continuously recording stations (triangles in Fig. 5.5), 106 short-period Mark L4 seismometers, 14 broadband Guralp seismometers, 8 ocean bottom hydrophones (OBH) and 6 ocean bottom seismometers (OBS), covered a region of about 150×200 km. OBHs and OBSs were deployed during the RV SONNE cruise SO176 to extend the land network offshore to the south of Central Java. The average onshore station spacing was ~ 20 km. The spacing of ocean bottom instruments was ~ 40 – 90 km. The seismic instruments recorded both the natural local earthquakes as well as airgun-generated shots, the latter generated during a second cruise (SO179) in September and October 2004. The interpreted amphibious data consisted of 50,060 first arrival travel-time picks of airgun shots fired along three seismic wide-angle profiles and recorded also with the onshore MERAMEX network. Four to five local earthquake events could be recorded per day, in addition to regional and teleseismic events. The clearest signals were observed in the southern and northern coastal areas. In Central Java, north of Merapi and Lawu, the recorded shear wave phases were strongly attenuated. Thus, even a preliminary qualitative evaluation of the seismograms showed that there is a significant seismic anomaly located beneath Central Java.

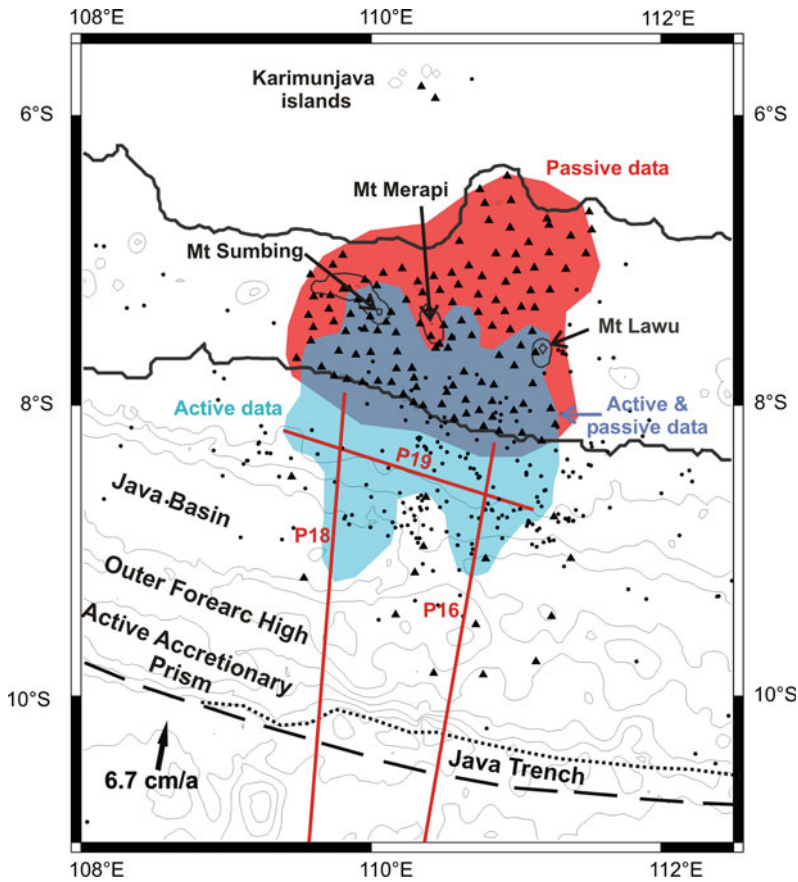


Fig. 5.5 Study area of the MERAMEX project, including the tectonic regime of the region. Triangles mark the temporary seismological network installed in 2004. Dots are recorded earthquakes collected in the MERAMEX catalogue. Red lines indicate seismic airgun profiles. The red coloured area in Central Java marks the area covered by passive seismic data, while the light blue and grey areas are covered by active seismic data and both data

For the earthquake data analysis, a total of 13,800 phases (8000 P- and 5800 S-phases) were selected for a simultaneous iterative source location and tomographic inversion. A detailed description of this study can be found in Koulakov et al. (2007, 2009b). The P velocity reference model down to a depth of 20 km was estimated based on results of an active seismic experiment performed in the offshore part of MERAMEX (Wagner et al. 2007a, b; Wittwer et al. 2010). For deeper parts, the velocity model was defined based on the global AK135 model

sets, respectively, in the uppermost 10 km depth layer. These areas are identified as areas with satisfactory recovery of 30 km size checkerboard anomalies at a depth of 5 km. The dotted line marks the current track of the Java trench, which is retreating northward from the normal curvature trend (dashed line) in front of Central Java (Wagner et al. 2007a)

(Kennett et al. 1995) because no reliable constraints were available for the range below 20 km depth. Derived final earthquake locations line up along the Wadati-Benioff Zone, but the events depict variable dipping angles of the slab. Looking to the north, for the first 150 km distance from the trench, the slab appears to be almost horizontal. From 250 to 450 km along profile P1–P2, the dip angle of the slab is about 45°, while in the depth interval from 250 to 600 km, the slab steepens to ~70° (Koulakov et al. 2007).

We developed new models of the anisotropic structure beneath central Java based on the local earthquake tomography (Koulakov et al. 2009b) (Figs. 5.6 and 5.7). Relative P (V_p) and S (V_s) velocity anomalies are illustrated in horizontal and vertical sections. The reconstruction of relative anomalies even in highly heterogeneous areas was fairly stable and found not to be significantly dependent on the chosen reference model (Koulakov et al. 2007). An interpretable spatial resolution could be achieved down to a depth of 150 km.

The first striking feature in the derived tomographic images is an almost perfect correlation of P and S wave anomalies in the crust. The most prominent feature in the crust is a strong low-velocity anomaly. This low-velocity anomaly is named Merapi-Lawu Anomaly (MLA), with a reduction in velocity up to 30% for the P-model, and up to 36% in case of the S-model. The MLA fills the areas within the main volcanic complexes

in Central Java. The largest part of this anomaly is located close to the volcanoes Merapi and Merbabu (briefly called “Merapi complex”), and extends to Lawu volcano at the eastern border of the investigation area. The second, smaller part lies between the Merapi complex and the volcanoes Sumbing, Sundoro and Dieng (briefly called “Sumbing complex”). Interestingly, these active volcanoes are not located above the central part of the anomaly but appear to be arranged surrounding it. In other words, the active volcanoes are found just above the contact region between the low-velocity anomaly and the high-velocity forearc. In vertical sections (Fig. 5.7), it is recognisable that the MLA is inclined southwards towards the subducting slab, extending into the upper mantle with decreasing intensity. The reliability of these models was tested comprehensively by Koulakov et al. (2007, 2009b).

Furthermore, the obtained seismic anomalies were compared with Bouguer gravity anomalies

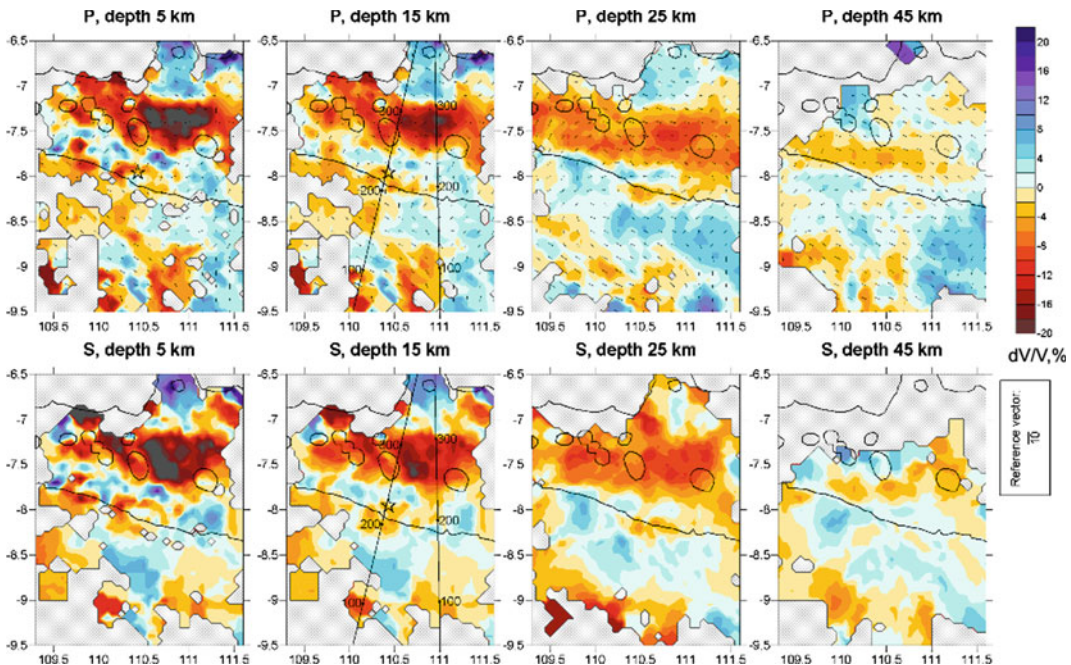


Fig. 5.6 Results of the anisotropic inversion after five iterations in horizontal sections. Colours indicate the isotropic velocity perturbations which are computed as an average of four anisotropic parameters in each point. Bars show directions of fast horizontal P velocities. The length of the bars reflects the difference between the fastest and

slowest horizontal velocities. The reference bar (10% of anisotropy) is shown in the right-bottom corner. Positions of two cross sections presented in Fig. 5.7 are marked in maps corresponding to 15 km depth. The star shows the hypocentre of the Bantul Mw = 6.4 earthquake on 26 May 2006 (UTC)

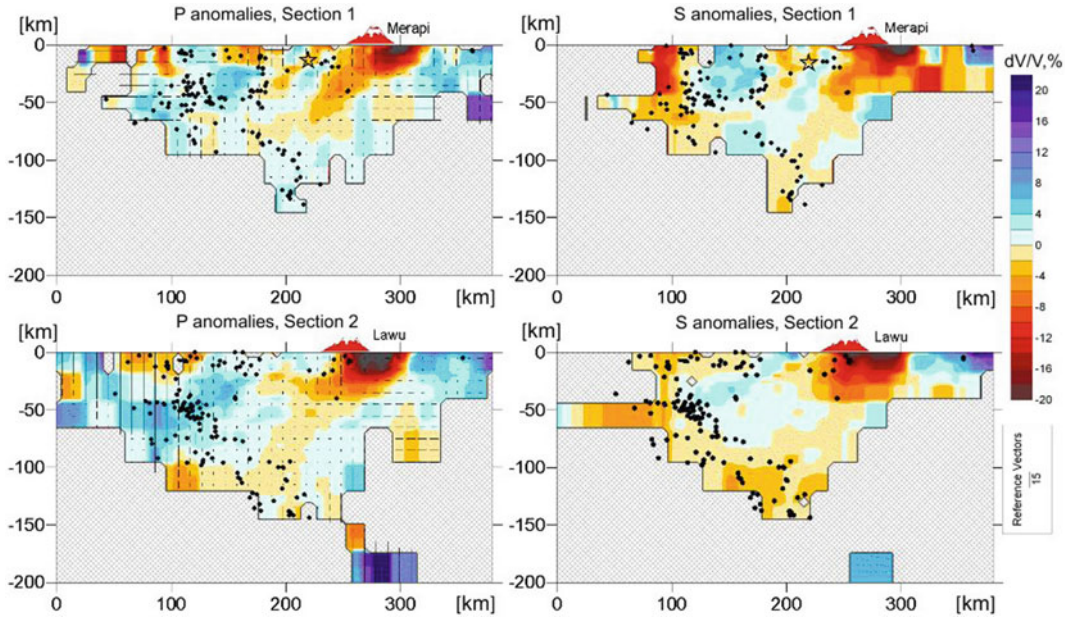


Fig. 5.7 Resulting anisotropic P and isotropic S models after five iterations in vertical sections. Positions of sections are shown in the map related to 15 km depth (Fig. 5.6). The anisotropy bars for the P model are vertical, if the vertical velocity variations are larger than

the average horizontal perturbations, and horizontal in the opposite case. The reference bar (6% of anisotropy) is shown in the left-bottom corner. The star shows the hypocentre of the Bantul Mw = 6.4 earthquake on 26 May 2006 (UTC)

(Sato 1978; Smith and Sandwell 1997), as illustrated in Fig. 5.8. It can be seen that the main features of gravity and seismic velocity models are consistent with each other. For example, the strong negative seismic anomaly located north of

the MLA corresponds to a negative gravity anomaly in the back-arc. Dominantly positive seismic anomalies in the forearc correspond to positive gravity anomalies. To quantify this link, we performed gravity modelling intended to

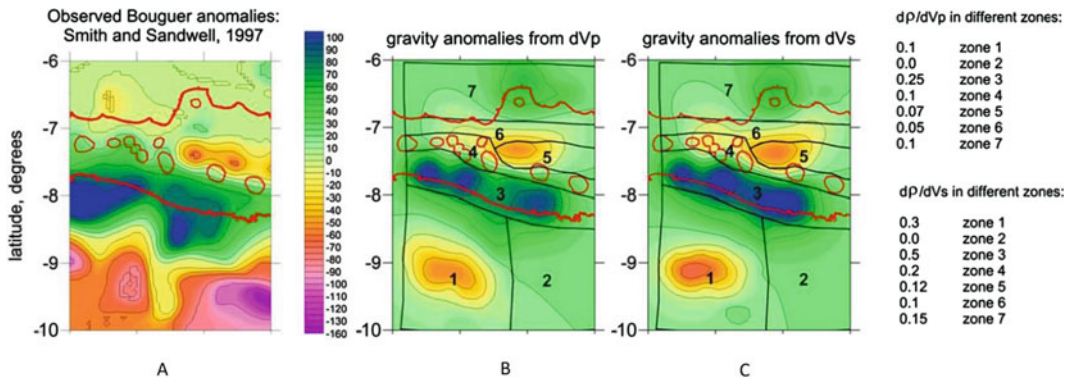


Fig. 5.8 Result of optimisation for dp/dv coefficients in the crust. The gravity map after Smith and Sandwell (1997) on the left and the calculated gravity values derived from Vp and Vs velocities (on the right) indicate a

strong negative gravity anomaly in Central Java, extending to the east. The gravity anomaly fits well with the Merapi-Lawu seismic velocity anomaly (centred at approximately 7°S, 111°E)

estimate values of dp/dv coefficients (anomalies of density over anomalies of seismic velocity) for different crustal zones.

For the gravity modelling, the crust was divided into several zones, representing main geological and geophysical features (Koulakov et al. 2007). The final computed gravity fields derived from the P- or S-velocity anomalies are shown in Fig. 5.8b, c. Although the derived coefficients determined by this modelling are not expected to be highly accurate, they provide semi-quantitative information concerning geological processes in the crust of Central Java. For the arc anomalies and the MLA, the calculated dp/dv values are found to be rather low (Koulakov et al. 2007, 2009b; Luehr et al. 2013).

Syracuse and Abers (2006) analysed the variations in vertical distance between arc volcanoes at the surface and the subducted slab at depth for nearly all subduction zones. They found that at subduction volcanoes, the average slab surface distance is ~ 100 km. Discrepancies were found only in a few cases, such as in Central Java, where the vertical distance from the surface to the slab is ~ 150 km. The authors attempted to explain such deviations from the average depth by calling on specific physical conditions. Another common feature of a subduction zone is that the earthquake hypocentre distributions show two maxima in depth. A shallow clustering at ~ 20 – 50 km is interpreted to be related to tectonic stress release. Another increase in the frequency of earthquakes can be detected at a depth range of ~ 100 km on average (International Seismological Centre 2001). These peaks in seismicity are also observable in the same depth ranges in the Sunda arc (Luehr et al. 2013; Halpaap et al. 2019).

The increase in seismicity in the range of 100 km depth can be explained by mineralogical phase transitions resulting in dehydration processes (e.g., Paulatto et al. 2017; Cooper et al. 2020) caused by de-serpentinisation, which leads to a volume decrease expressed by earthquakes (Davey and Ristau 2011).

Mineralogical investigations of Mierdel et al. (2007) demonstrated that the ratio of water saturation versus depth has a pronounced minimum

at depths between 100 and 200 km (Bolfan-Casanova 2007). Depending on the tectonic environment and temperature, the minimum solubility may be shallow, as in the case of the oceanic mantle, but deeper in the case of cold continental lithosphere. We propose that in the case of Central Java at a depth range near 100 km, where seismicity is increased, fluids (mainly water) are released from the subducted slab and begin to ascend into the overlying mantle wedge, leading to a reduction in melting temperature of the mantle rock (e.g., Poli and Schmidt 1995). The ascent path of upward migrating fluids released from the slab is imaged tomographically as a zone of low seismic velocity (Koulakov et al. 2007). In the case of Central Java, this path is not vertical but inclined at 45° and oriented towards the trench (Fig. 5.7). The ascending fluids cause decreasing viscosity and partial melting of the mantle. The melts then penetrate the arc crust and form magma reservoirs in the lower and middle crust and, in some cases, rise to the surface and cause volcanic eruptions.

As shown above, the most important feature of the MERAMEX tomographic models is an unusually strong low-velocity anomaly located in the backarc crust just north of the volcanoes Sumbing, Merapi and Lawu (Figs. 5.6 and 5.7). The main part of this anomaly extends for ~ 80 km from east to west and ~ 30 km from north to south, and to a depth of >50 km, from where it further extends as an inclined tongue with decreasing amplitude towards the slab pointing at a depth of ~ 100 km. The active volcanoes are located at the edge of this anomaly between high and low-velocity regions. Considering this geometry, it can be estimated that the low-velocity body has a volume of $>50,000$ km³ characterised by a reduction in velocity of up to 20% for the seismic P-wave model and up to 25% for the S-wave model (Koulakov et al. 2007, 2009b). Shear wave signals recorded above this zone are strongly attenuated compared to areas outside the anomaly volume. Furthermore, there is a good correlation between the distribution of velocity anomalies in the crust and gravity anomalies. High-velocity seismic

anomalies in the forearc correspond to gravity highs and the low-velocity MLA matches well with a distinct gravity low corresponding to the Kendeng Basin, which is located north of the MLA and parallel to the volcanic front of Central and East Java (Koulakov et al. 2007). The Kendeng Basin succession is not well exposed but contains much volcanic debris (see Harijoko et al. 2023, Chap. 4). The deposits have an estimated thickness of up to 10 km based on gravity modelling (Waltham et al. 2008). Consequently, we interpret this behind-the-volcanic-front anomaly as the combined product of a thick package of low-velocity sediments in the upper crust, and increased temperatures and magmatic fluids in the middle and lower crust. The very low P- and S-velocities within the shallowest part of the MLA could in part result from a high fluid (gas and liquid) content in the sediment layers. Mud volcanoes in northern Central Java (Satyana and Asnidar 2008), which actively release methane, favour this hypothesis. Synthetic tests (Koulakov et al. 2007) confirmed that the MLA cannot be explained simply and requires that the lower crust must also have low velocities, as confirmed by active seismic studies (Wagner et al. 2007b).

The velocity perturbations, attenuation of P- and S-waves, and high V_p/V_s ratio of the MLA, indicating a high Poisson's ratio of 0.3 and matching with a gravity low, suggest an area of increased temperature and reduced shear strength in the crust. Depending on the elastic modulus, a fluid and partial melt amount of 13–25% can be estimated for the MLA volume. Assuming that the region of the MLA beneath the sedimentary basin consists of a rigid matrix with cells filled with a magmatic crystal mush or near-molten material, the sediments may act as a seal for fluids from the mantle wedge just beneath the MLA to move vertically towards the surface. This hypothesis is indirectly supported by relatively strong, randomly looking travel time residuals after inversion (Koulakov et al. 2007). An explanation for this noise could be the existence of relatively small bodies of contrasting material, causing scattering (Luehr et al. 2013). These may affect the travel times of seismic rays

but cannot be resolved by the tomographic inversion. Considering realistic frequencies of seismic signals from natural sources, a significant scattering-induced effect on the travel time can be expected only for anomalies of a minimum diameter of 1–2 km. Anomalies of 15–20 km extension, for instance, would be resolved in the images clearly and would lead to more coherent signals. Therefore, the lower part of the MLA can be interpreted as a zone composed of a solid matrix or may be a 'reservoir' similar to a sponge structure that contains cells or sheeted sill structures of 2–15 km diameter filled with molten or partially molten material. This hypothesis is supported by petrological findings of magma storage and crystallisation at Merapi (e.g., Chadwick et al. 2013; Costa et al. 2013; Deegan et al. 2016; Preece et al. 2016; Peters et al. 2017; Troll and Deegan 2023, Chap. 8). Furthermore, Merapi magmas are contaminated by carbonates from the subvolcanic basement derived from depth of 3–11 km (e.g., Chadwick et al. 2007, 2013; Deegan et al. 2010, 2023; Chap. 10; Whitley et al. 2020). A significant contribution to the magmatic volatile budget via limestone assimilation may therefore influence the driving mechanism of eruptions at Merapi and other volcanoes sited on carbonate crust (e.g., Troll et al. 2012; Blythe et al. 2015; Deegan et al. 2023; Chap. 10).

The degree of velocity anomalies found beneath Central Java is exceptional, when compared to anomalies found at other subduction zones and large volcanic systems. For example, Toba volcano in northern Sumatra is the source of the largest eruption on Earth within the last two million years. The resulting caldera is 30×100 km wide and has a total relief of 1700 m. In one eruptive phase 75,000 year ago, Toba produced the Youngest Toba Tuff, which has an estimated volume of 2800 km^3 (e.g., Chesner and Rose 1991). Tomographic investigations of the Toba area (Koulakov et al. 2009a) derived a model that images patches of negative anomalies beneath Toba with velocity reduction values of no more than 15%. Such a velocity reduction appears to be typical for volcanic areas at subduction zones and is comparable to

anomalies found in the Andes (Schurr et al. 2003; Koulakov et al. 2005) and Kamchatka (Koulakov et al. 2011).

5.5.2 Shallower Structure Beneath Merapi

The resolution of our local earthquake tomography method using P- and S-body waves decreases with decreasing crustal depth. To improve the resolution in the shallower crust, especially in the uppermost 5 km, a tomographic inversion might be realised from the analysis of ambient noise data. Different levels of anomalies, which were previously blurred and indistinguishable in the Local Earthquake Tomography (LET) results (Koulakov et al. 2009b), can now be separated by applying the Ambient Noise Tomography (ANT) modelling method.

Results of ANT modelling for the MER-AMEX data in the Central Java area by Koulakov et al. (2016) show strong variations in the S-wave velocity, especially at shallow depths. Between the coastline and the volcanoes Merapi and Lawu, the authors found a strong high-velocity anomaly with an amplitude exceeding 25%. Beneath and to the south of Merapi, strong negative anomalies were revealed with amplitudes that reached -25% . Thus, the variations derived with this tomographic method are of the same order of magnitude as those of previous tomographic studies based on travel time tomography (Koulakov et al. 2007, 2009b). In Fig. 5.9, the ANT modelling results are compared with the results of the model derived from LET (Koulakov et al. 2009b). The main features, such as the high-velocity forearc and low-velocity anomalies surrounded by the volcanoes in Central Java, appear similar in both models. However, there are subtle differences. For example, in the LET results, the most prominent low-velocity anomaly has a high magnitude across the entire area between Merapi and Lawu, whereas in the ANT model, the eastern part of the anomaly in the vicinity of Lawu volcano is less pronounced. This difference can be partly explained by the lower resolution of the ANT

model in the eastern area of investigation and by some leakage of the amplitude of anomalies (Koulakov et al. 2016). Also, it has to be noted that the LET results were affected by significant vertical smearing, which suggests that some differences between the models may be caused by the projection of anomalies from different depths. For the vertical section (Fig. 5.9b, d), an overall fit of the main anomalies is observable in both the LET and ANT models. In the ANT model, an anomaly beneath the Merapi cone is apparent, whereas in the LET model, this shallow anomaly is not apparent. Interestingly, a large anomaly at the bottom-left corner of the ANT section is consistent with the inclined low-velocity anomaly in the LET model that links the volcano-related structures with the subducting slab. According to the results of the ANT model, the low-velocity anomaly beneath the northern flank of Merapi (section A1–B1; Fig. 5.9b) seems to be separated into two parts. Koulakov et al. (2016) suggested that the upper portion of this anomaly represents a thick layer of volcanoclastic sediments accumulated over a long period of time. Based on this model, the thickness of this layer may be greater than 1 km. A second strong low-velocity anomaly, detected at depths between 4 and 8 km beneath this volcanoclastic sediment layer, may be associated with a large, shallow felsic magma reservoir, as proposed by Koulakov et al. (2009b) based on the results of the LET model, and demonstrated by horizontally oriented anisotropy that may indicate a sill structure of this reservoir. A similar sill structure for a felsic magma reservoir at a similar depth range was identified beneath the Toba caldera (Jaxybulatov et al. 2014). However, it is notable that this structure appears to be separated from the upper crustal anomalies, although the ANT model tends to shift the deep boundaries higher. Consequently, the real location of this anomaly may be deeper than is indicated by these particular results.

A separation of two low-velocity layers is also found by the latest larger structure investigation project DOMERAPI. Within this project, a much denser seismic network of 46 broad-band seismometers was installed around Merapi between

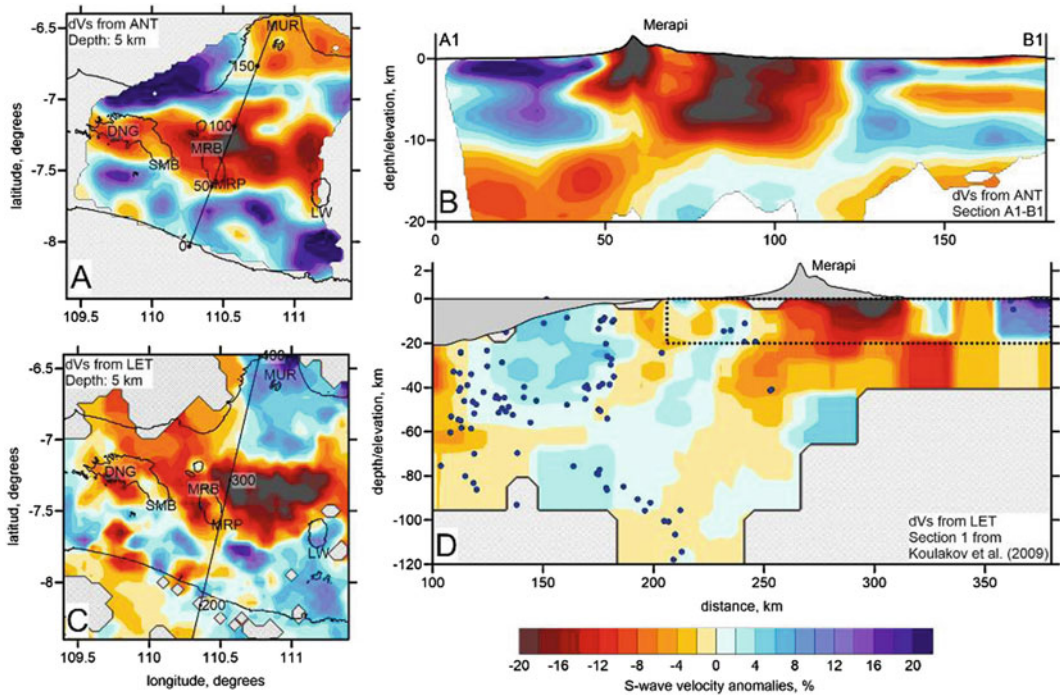


Fig. 5.9 Comparison of the ambient noise tomography (ANT) with the body wave local earthquake tomography model (LET). **a** and **c** are horizontal sections at 5 km depth of the ANT and LET model, respectively. Contour lines of topography at 1000 m altitude are shown with black lines. **b** and **d** are the vertical sections of the ANT and LET models along the profiles indicated in figures

a and **b**. In **b**, the vertical scale is twice exaggerated for positive altitudes. Blue points in **d** show earthquake hypocentres. The dotted line in **d** depicts the area corresponding to the section in **b**. The exaggerated topography for positive altitudes along the profiles is presented in images **b** and **d**

October 2013 and mid-April 2015 (Widiyantoro et al. 2018). The stations were deployed with an inter-station distance of ~ 4 km and the DOMERAPI data were combined with data of the permanent BMKG. All detected seismic events were relocated using a double-difference earthquake location algorithm. The jointly processed data produced a new, high-quality catalogue comprising 358 events for imaging the V_p and V_p/V_s structure below Merapi in exceptional detail, from below the volcano's summit to a depth of ~ 20 km below sea level. The P- and S-wave arrival time data with similar path coverage reveal a high V_p/V_s structure extending vertically from a depth of ≥ 20 km bsl up to the summit of Merapi. As mentioned by Koulakov et al. (2016) and Widiyantoro et al. (2018), their tomographic inversions reveal two pronounced anomalies beneath Merapi. One anomaly located

at <4 km depth was demonstrated by low V_p and very low V_s values as well as high V_p/V_s ratios. A second anomaly was found at ~ 10 – 20 km depth, with high V_p , very low V_s values and very high V_p/V_s ratios. Interestingly, their V_p/V_s tomograms suggests that another deeper anomaly may exist near the MOHO at ≥ 25 km depth with low V_p and low V_s values as well as high V_p/V_s ratios that match the findings of the MERAMEX project of a very large anomaly in Central Java with an estimated volume of more than $50,000$ km³ (Koulakov et al. 2007; Luehr et al. 2013). However, the most denoting feature in their tomographic images is a distinct sub-vertical high V_p/V_s anomaly. If this finding is correct, this sub-vertical, high V_p/V_s anomaly outlines a fluid-rich zone and, therefore, the last part of the magma ascent path from a depth of ~ 20 km up to the surface.

It is noteworthy that volcano edifices are typically associated with higher seismic velocities at the shallowest depths, representing the rigid properties of highly consolidated igneous rocks, whereas in areas between volcanoes, shallow seismic anomalies are generally negative. These negative anomalies can be explained by volcanoclastic deposits, eroded and transported down the volcano flanks by lahars and rivers. During the Bantul earthquake in May 2006, such deposits showed devastating effects, when strong resonant shaking with relatively high frequencies led to severe destruction of mainly smaller buildings and caused >5700 fatalities (e.g., Walter et al. 2008).

5.6 Summary

The past 25 years of investigation of the volcanism and magmatism of Merapi and the surrounding area in Central Java have brought geological and geophysical advances that greatly helped define the structure of the magma plumbing system and underlying magmatic processes. Direct current electrical resistivity (DC) tomography and magnetotelluric (MT, LOTEM) investigations as well as gravity measurements revealed the highly complex resistivity and density structure of the Merapi edifice and have provided many geophysical parameters that led to an improved understanding of the volcano's hydrological and hydrothermal system and its dynamics. The highly sensitive borehole tiltmeter array measurements on the flanks showed very small signal values related to Merapi's activity in 1997 and 1998 only, with a tilt signal of maximum $1 \mu\text{rad}$ associated with the 14 January 1997 explosive event. Many of the results obtained pertain to the large area between the subducting slab and the summit area and are not only valid for Merapi, but may also apply to other subduction zone volcanoes. A schematic cartoon illustrating the processes taking place beneath Central Java is shown in Fig. 5.10. As proposed by Luehr et al. (2013), an increased

level of subducted slab-related seismicity in Central Java can be observed at ~ 100 km depth, which likely represents dehydration and the release of hydrous volatiles from the slab (e.g., Peacock 1990; Maruyama and Okamoto 2007). When these volatiles pass through the mantle wedge, they react with the mantle rock and lower its melting temperature (e.g., Poli and Schmidt 1995) and the seismic velocity. In the case of Central Java, the ascent of fluids and partial melts is not vertical but inclined to the north. At the base of the crust at a depth of ~ 38 km (Wölbner and Rumpker 2016), a remarkable large negative velocity anomaly was detected by tomographic imaging, hinting at a large amount of partially molten rock and volatiles. Volcanoes at the surface in Central Java are located at the boundary of this anomaly. As suggested by Shapiro and Koulakov (2015), the continental crust may become a barrier for magmas from the mantle. Magma may ascend through the lower mafic crust but cannot propagate further into the upper felsic crust because of insufficient buoyancy. The low-velocity anomaly at ~ 20 km depth, which is separated from anomalies in the upper crust, may represent the top of the mafic magma pathway at the boundary between the lower and upper crust. Meanwhile, volatiles may continue to rise, providing substantial heat, partial melts and fluids from the mantle wedge, and may cause crustal assimilation in the upper crust (e.g., Deegan et al. 2023, Chap. 10). Fluids and partially molten material are inferred to form a complex system of reservoirs that feed Merapi's eruptions, as imaged by V_p/V_s ratio anomalies at depths <4 km and between 10 and 20 km. This derived geophysical image of the plumbing system of Merapi, with three main reservoirs along the magma ascent path is still simplified but consistent with petrological findings recorded in minerals as well as plutonic and crustal inclusions for the same depth ranges (Troll and Deegan 2023, Chap. 8) that also suggest the presence of significant portions of crystal mush.

For the Merapi edifice, a surprising result has been that seismic signals are affected by a strong

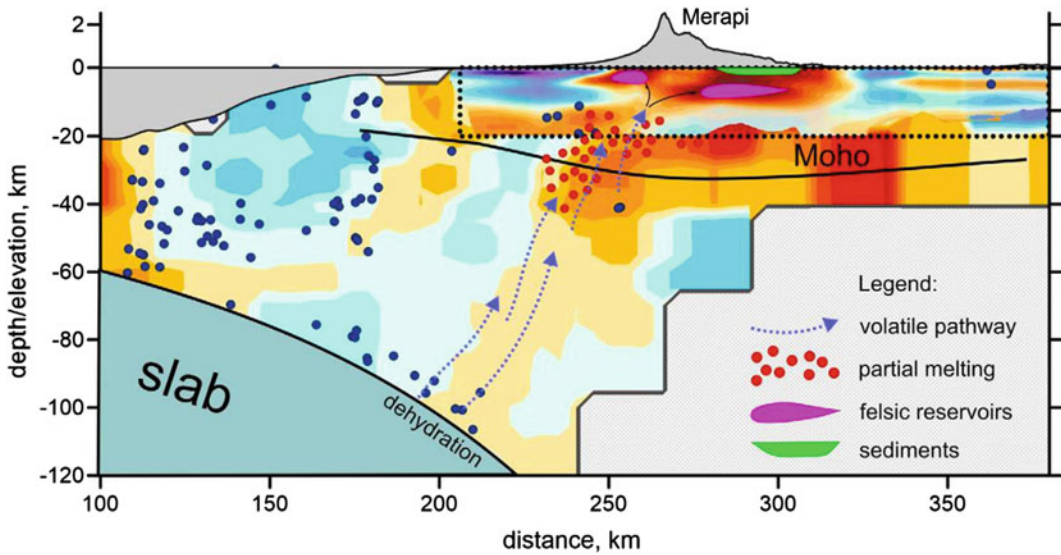


Fig. 5.10 Overlapped results of the LET and ANT models in a vertical section, as shown in Fig. 5.9d, and possible interpretation. Exaggerated topography is shown for positive altitudes. The Moho interface is schematically

indicated according to Wölbern and Rumpker (2016). Blue dots are earthquakes. The grey area depicts the subducting slab (after Koulakov et al. 2016)

scattering effect, caused by the heterogeneous construction of such a volcano. At Merapi, the mean free pathway for higher frequent signals is statistically only 100 m. This means that a generated signal will be affected by multiple scattering after travelling a distance of 100 m and, particularly, that the first onset amplitude is fading. Before the recent findings, seismic signals such as multiphase events were commonly explained by a complex seismic source mechanism of these volcanic earthquakes. However, as a result of this recent work, an alternative model has been established, highlighting those complex signals of volcanic earthquakes can also be explained by multiple scattering effects on their path within a stratovolcano. This effect on seismic waves is probably valid for many similar active volcanoes at subduction zones elsewhere. Moreover, inside this uppermost part of the Merapi edifice, a hydrothermal zone could be detected that surrounds the shallow volcanic conduit. The permeability of this zone up to the summit lava dome is not constant in time as recently shown by Heap et al. (2019). Highly mineralised fluids and gases that pass through

this zone lead to precipitation of sulphur and other minerals in pores and fractures that reduce the permeability of the host rock. This may result in a pressure increase in the conduit system with important implications for the eruptive activity and hazard assessment.

Acknowledgements The authors are grateful to get support for the different research projects by many colleagues and institutions. Funding was provided by the German Science Foundation (DFG), GeoForschungsZentrum Potsdam (GFZ) and the Volcanological Survey of Indonesia (VSI). Support by UNESCO, Deutsche Gesellschaft für Technische Zusammenarbeit (GTZ) and the International Bureau of German Federal Ministry for Education and Research (BMBF) is gratefully acknowledged. For scientific and logistical support, we are very grateful to our Indonesian partners from the former VSI in Bandung, Badan Meteorologi Klimatologi dan Geofisika (BMKG) in Jakarta, Gadjah Mada University (UGM) in Yogyakarta and the Institut Teknologi Bandung (ITB) in Bandung. Without the enthusiastic help of the Indonesian students these projects could not have been realised. We are also thankful that Ivan Kulakov could be supported by the RSF Grant #20-17-00075. Last but not least, the authors would like to thank the reviewers, especially Ralf Gertisser, Valentin Troll, Thomas Walter and Sri Widiyantoro. Their valuable help and guidance improved the quality of this chapter enormously.

References

- Beauducel F, Cornet FH (1999) Collection and three-dimensional modeling of GPS and tilt data at Merapi volcano. *Java. J Geophys Res* 104(B1):725–736
- van Bemmelen RW (1949) *The geology of Indonesia*, vol 1A. General Geology, Government Printing Office, The Hague, p 732
- Blythe LS, Deegan FM, Fred C, Jolis RM, Masotta M, Misiti V, Taddeucci J, Troll VR (2015) CO₂ bubble generation and migration during magma–carbonate interaction. *Contrib Mineral Petrol* 169:42
- Bohm M, Asch G, Fauzi F, Flüh ER, Brotopuspito KS, Kopp H, Luehr B-G, Puspito NT, Ratdomopurbo A, Rabbel W, Wagner D, MERAMEX Research Group (2005) The MERAMEX project—a seismological network in Central Java, Indonesia. *GEOTECHNOLOGIEN Science Report 5*, ‘Continental Margins—Earth’s Focal Points of Usage and Hazard Potential’, Potsdam, Germany
- Bolfan-Casanova N (2007) Fuel for plate tectonics. *Science* 315:338–339
- Budi-Santoso A, Beauducel F, Nandaka IGMA, Humaida H, Costa F, Widiwijayanti C, Iguchi M, Métaxian J-P, Rudianto I, Rozin M, Sulistiyani, Nurdin I, Kelfoun K, Byrdina S, Pinel V, Fahmi AA, Laurin A, Rizal MH, Dahamna N (2023) The Merapi volcano monitoring system. In: Gertisser R, Troll VR, Walter TR, Nandaka IGMA, Ratdomopurbo A (eds) *Merapi volcano—geology, eruptive activity, and monitoring of a high-risk volcano*. Springer, Berlin, Heidelberg, pp 409–436
- Budi-Santoso A, Lesage P (2016) Velocity variations associated with the large 2010 eruption of Merapi volcano, Java, retrieved from seismic multiplets and ambient noise cross-correlation. *Geophys J Int* 206:221–240
- Byrdina S, Friedel S, Vandemeulebrouck J, Budi-Santoso A, Suhari SW, Rizal MH, Winata E, Kusdaryanto (2017) Geophysical image of the hydrothermal system of Merapi volcano. *J Volcanol Geotherm Res* 329:30–40
- Chadwick JP, Troll VR, Ginibre C, Morgan D, Gertisser R, Waight TE, Davidson JP (2007) Carbonate assimilation at Merapi volcano, Java, Indonesia: insight from crystal isotope stratigraphy. *J Petrol* 48:1793–1812
- Chadwick JP, Troll VR, Waight TE, van der Zwan FM, Schwarzkopf LM (2013) Petrology and geochemistry of igneous inclusions in recent Merapi deposits: a window into the sub-volcanic plumbing system. *Contrib Mineral Petrol* 165:259–282
- Chesner CA, Rose WI (1991) Stratigraphy of the Toba Tuffs and the evolution of the Toba Caldera Complex, Sumatra, Indonesia. *Bull Volcanol* 53:343–356
- Commer M, Helwig SL, Hördt A, Tezkan B (2005) Interpretation of long-offset TEM data from Mount Merapi (Indonesia) using a 3D optimization approach. *J Geophys Res* 110:B03207
- Commer M, Helwig SL, Hördt A, Scholl TB (2006) New results on the resistivity structure of Merapi Volcano (Indonesia), derived from 3D restricted inversion of long-offset transient electromagnetic data. *Geophys J Int* 167:1172–1187
- Cooper GF, Macpherson CG, Blundy JD, Maunder B, Allen RW, Goes S, Collier JS, Bie L, Harmon N, Hicks SP, Iveson AA, Prytulak J, Rietbrock A, Rychert CA, Davidson JP, The VoiLA Team (2020) Variable water input controls evolution of the Lesser Antilles volcanic arc. *Nature* 582:525–529
- Costa F, Andreatuti S, Bouvet de Maisonneuve C, Pallister J (2013) Petrological insights into the storage conditions, and magmatic processes that yielded the centennial 2010 Merapi explosive eruption. *J Volcanol Geotherm Res* 261:209–235
- Dainty AM, Toksöz MN (1981) Seismic codas on the earth and the moon: a comparison. *Phys Earth Planet Inter* 26(4):250–260
- Davey FJ, Ristau J (2011) Fore-arc mantle wedge seismicity under Northeast New Zealand. *Tectonophysics* 509:272–279
- Deegan FM, Troll VR, Freda C, Misiti V, Chadwick JP, McLeod CL, Davidson JP (2010) Magma-Carbonate Interaction Processes and Associated CO₂ Release at Merapi Volcano, Indonesia: insights from experimental petrology. *J Petrol* 51:1027–1051
- Deegan FM, Whitehouse MJ, Troll VR, Budd DA, Harris C, Geiger H, Hålenius U (2016) Pyroxene standards for SIMS oxygen isotope analysis and their application to Merapi volcano, Sunda Arc, Indonesia. *Chem Geol* 447:1–10
- Deegan FM, Troll VR, Gertisser R, Freda C (2023) Magma-carbonate interaction at Merapi volcano, Indonesia. In: Gertisser R, Troll VR, Walter TR, Nandaka IGMA, Ratdomopurbo A (eds) *Merapi volcano—geology, eruptive activity, and monitoring of a high-risk volcano*. Springer, Berlin, Heidelberg, pp 291–321
- Delcamp A, Wyk V, de Vries B, James MR (2008) The influence of edifice slope and substrata on volcano spreading. *J Volcanol Geotherm Res* 177:925–943
- Dzurisin D (2007) *Volcano deformation: new geodetic monitoring techniques*. Springer-Verlag, Berlin, Heidelberg
- Friedel S, Jacobs F, Flechsig C, Reißmann C, Brunner I (1998) Large-scale DC resistivity imaging at Merapi Volcano. *DGG-Mitt Spec Issue III(1998):35–40*
- Friedel S, Brunner I, Jacobs F, Rücker C (2000) New results from DC resistivity imaging along the flanks of Merapi volcano. *DGG-Mitt Spec Issue IV/2000:23–29*
- Gerstenecker C, Heinrich R, Jentzsch G, Kracke D, Läufer G, Suyanto I, Weise A (1998a) Microgravity at Merapi Volcano: Results of the first two Campaigns. *DGG-Mitt Spec Issue III(1998):61–64*
- Gerstenecker C, Läufer G, Snilil B, Wrobel B (1998b) Digital Elevation Models for Mount Merapi. *DGG-Mitteilungen, Special Issue III(1998):65–68*
- Gossler J, Kind R, Sobolev SV, Kämpf H, Wylegalla K, Stiller M, TOR Working Group (1999) Major crustal

- features from the Harz Mountains to the Baltic Shield derived from receiver functions. *Tectonophysics* 314 (1–3):321–333
- Gossler J (2000) Teleseismic observations at Merapi Volcano, Indonesia. *DGG-Mitt Spec Issue IV/2000*:17–22
- Halpaap F, Rondenay S, Perrin A, Goes S, Ottemöller L, Austrheim H, Shaw R, Eeken TH (2019) Earthquakes track subduction fluids from slab source to mantle wedge sink. *Sci Adv* 5(4):eaav7369
- Harijoko A, Marliyani GI, Wibowo HE, Freski YR, Handini E (2023) The geodynamic setting and geological context of Merapi volcano in Central Java, Indonesia. In: Gertisser R, Troll VR, Walter TR, Nandaka IGMA, Ratdomopurbo A (eds) Merapi volcano—geology, eruptive activity, and monitoring of a high-risk volcano. Springer, Berlin, Heidelberg, pp 89–109
- Heap MJ, Troll VR, Alexandra RL, Kushnir ARL, Gilg HA, Collinson ASD, Deegan FM, Darmawan H, Seraphine N, Neuberg J, Walter TR (2019) Hydrothermal alteration of andesitic lava domes can lead to explosive volcanic behaviour. *Nat Comms* 10:5063
- Hoffmann-Rothe A, Mueller A, Ritter O, Haak V (1998) Magnetotelluric Survey at Merapi Volcano and across Java, Indonesia. *DGG-Mitt Spec Issue III(1998)*:47–52
- International Seismological Centre (2001) On-line Bulletin. <https://doi.org/10.31905/D808B830>
- Jaxybulatov KNM, Shapiro M, Koulakov I, Mordret A, Landes M, Sens-Schoenfelder C (2014) A large magmatic sill complex beneath the Toba caldera. *Science* 346:617–619
- Kalscheuer T, Commer M, Helwig SL, Hördt A, Tezkan B (2007) Electromagnetic evidence for an ancient avalanche caldera rim on the south flank of Mount Merapi, Indonesia. *J Volcanol Geotherm Res* 162:81–97
- Kelfoun K (1999) Processus de croissance et de déstabilisation des dômes de lave du volcan Merapi (Java centrale, Indonésie): Modélisations numériques des dômes, dynamique des écoulements pyroclastiques associés et surveillance par stéréo-photogrammétrie. PhD Thesis, Université Blaise Pascal Clermont-Ferrand II, Clermont-Ferrand, France
- Keller GV (1988) Rock and mineral properties. In: Nabighian MC (ed) *Electromagnetic methods in applied geophysics: vol 1, Theory*. Society of exploration geophysicists, pp 13–52
- Kennett BLN, Engdahl ER, Buland R (1995) Constraints on seismic velocities in the Earth from traveltimes. *Geophys J Int* 122:108–124
- Koulakov I, Sobolev SV, Asch G (2005) P- and S-velocity images of the lithosphere asthenosphere system in the Central Andes from local-source tomographic inversion. *Geophys J Int* 167:106–126
- Koulakov I, Bohm M, Asch G, Luehr B-G, Manzanares A, Brotopuspito KS, Fauzi PMA, Puspito NT, Ratdomopurbo A, Kopp H, Rabbel W (2007) P and S velocity structure of the crust and the upper mantle beneath central Java from local tomography inversion. *J Geophys Res* 112:B08310
- Koulakov I, Yudistira T, Luehr B-G, Wandono (2009) P, S velocity and VP/VS ratio beneath the Toba caldera complex (Northern Sumatra) from local earthquake tomography. *Geophys J Int* 177:1121–1139
- Koulakov I, Jakovlev A, Luehr B-G (2009) Anisotropic structure beneath central Java from local earthquake tomography. *Geochem Geophys Geosyst* 10:Q02011
- Koulakov I, Gordeev EI, Dobretsov NL, Vernikovskiy VA, Senyukov S, Jakovlev A (2011) Feeding volcanoes of the Kluchevskoy group from the results of local earthquake tomography. *Geophys Res Lett* 38:L09305
- Koulakov I, Maksotova G, Jaxybulatov K, Kasatkina E, Shapiro NM, Luehr B-G, El Khrepy S, Al-Arifi N (2016) Structure of magma reservoirs beneath Merapi and surrounding volcanic centers of Central Java modeled from ambient noise tomography. *Geochem Geophys Geosyst* 17:4195–4211
- Lloyd JW, Pim RH, Watkins MD, Suwara A (2007) The problems of groundwater assessment in the volcanic-sedimentary environment of Central Java. *Q J Eng Geol Hydrogeol* 18(1):47–61
- Luehr B-G, Maercklin N, Rabbel W, Wegler U (1998) Active Seismic Measurements at the Merapi Volcano, Java Indonesia. *DGG-Mitt Spec Issue III(1998)*:53–56
- Luehr B-G, Koulakov I, Rabbel W, Zschau J, Ratdomopurbo A, Brotopuspito KS, Fauzi P, Sahara DP (2013) Fluid ascent and magma storage beneath Gunung Merapi revealed by multiscale seismic imaging. *J Volcanol Geotherm Res* 261:7–19
- Maercklin NC, Riedel C, Rabbel W, Wegler U, Luehr B-G, Zschau J (2000) Structural Investigation of Mt. Merapi by an Active Seismic Experiment. *DGG-Mitt Spec Issue IV/2000*:13–16
- Maruyama S, Okamoto K (2007) Water transportation from the subducting slab into the mantle transition zone. *Gondwana Res* 11(1):148–165
- Mierdel K, Keppler H, Smyth JR, Langenhorst F (2007) Water solubility in aluminous orthopyroxene and the origin of Earth's asthenosphere. *Science* 315:364–368
- Müller A, Haak V (2004) 3-D modeling of the deep electrical conductivity of Merapi Volcano (Central Java): integrating magnetotellurics, induction vectors and the effects of steep topography. *J Volcanol Geotherm Res* 138:205–222
- Müller M, Hördt A, Neubauer FM (1998) The LOTEM survey at Merapi Volcano 1998. *DGG-Mitt Spec Issue III/1998*:41–46
- Müller M, Hördt A, Neubauer FM (2002) Internal structure of Mount Merapi, Indonesia, derived from long-offset transient electromagnetic data. *J Geophys Res* 107(B9):ECV 2–1–ECV 2–14
- Müller M (2000) *Elektromagnetik an Vulkanen*. PhD Thesis, Universität zu Köln, Köln, Germany
- Nandaka IGMA (1999) Étude des déformations d'un volcan actif à dôme. Application au Merapi. DEA Report, Institut de Physique du Globe de Paris, France

- Paulatto M, Laigle M, Galve A, Charvis P, Sapin M, Bayrakci G, Evain M, Kopp H (2017) Dehydration of subducting slow-spread oceanic lithosphere in the Lesser Antilles. *Nat Comms* 8:15980
- Peacock SA (1990) Fluid processes in subduction zones. *Science* 248:329–337
- Peters STM, Troll VR, Weis FA, Dallai L, Chadwick JP, Schulz B (2017) Amphibole megacrysts as a probe into the deep plumbing system of Merapi volcano, Central Java Indonesia. *Contrib Mineral Petrol* 172:16
- Poli S, Schmidt MW (1995) H₂O transport and release in subduction zones: experimental constraints on basaltic and andesitic systems. *J Geophys Res* 100:22299–22314
- Preece K, Barclay J, Gertisser R, Herd RA (2013) Textural and micro-petrological variations in the eruptive products of the 2006 dome-forming eruption of Merapi volcano, Indonesia: implications for subsurface processes. *J Volcanol Geotherm Res* 261: 98–120
- Preece K, Gertisser R, Barclay J, Charbonnier SJ, Komorowski J-C, Herd RA (2016) Transitions between explosive and effusive phases during the cataclysmic 2010 eruption of Merapi volcano, Java, Indonesia. *Bull Volcanol* 78:54
- Purbawinata MA, Ratdomopurbo A, Sinulingga IK, Sumarti S, and Suharno (eds) (1997) Merapi Volcano—a guide book. *Volcanol Surv Indon*, Bandung, Indonesia, p 64
- Ratdomopurbo A, Poupinet G (1995) Monitoring temporal change of seismic velocity in a volcano: application to the 1992 eruption of Mt. Merapi (Indonesia). *Geophys Res Lett* 22(7):775–778
- Ratdomopurbo A (1995) Etude sismologique du volcan Merapi et formation du dome de 1994. Ph.D. Thesis Université Joseph Fourier, Grenoble, France
- Rebscher D, Westerhaus M, Körner A, Welle W, Nandaka GM (2000a) Monitoring ground deformation at the Decade Volcano Gunung Merapi Indonesia. *Phys Chem Earth Int* 25(9–11):755–757
- Rebscher D, Westerhaus M, Körner A, Welle W, Subandriyo, Brodscholl A, Kumpel H-J, Zschau J (2000b) Indonesian-German multiparameters stations at Merapi Volcano. *DGG-Mitt Spec Issue IV/2000b*:93–102
- Reichert C, Lühr B-G (2005) High risk volcanism at the active margin of the SUNDA ARC -BMBF GEOTECHNOLOGIEN Science Report 5, 'Continental Margins—Earth's Focal Points of Usage and Hazard Potential.' Potsdam, Germany
- Ritter O, Hoffmann-Rothe A, Müller A, Dwipa S, Arsadi E, Mahfi A, Nurnusanto I, Byrdina S, Echternacht F, Haak V (1998) A magnetotelluric profile across Central Java Indonesia. *Geophys Res Lett* 25 (23):4265–4268
- Sato Y (1978) Gravity and geological studies in Java, Indonesia. Geological survey of Indonesia and geological survey of Japan joint research program on regional tectonics of Southeast Asia. Geological Survey of Indonesia, p 207
- Satyana AH, Asnidar (2008) Mud diapirs and mud volcanoes in depressions of Java to Madura: origins, nature, and implications to petroleum system. In: Proceedings of the 32nd annual convention and exhibition of the Indonesian petroleum association, IPA08-G-139
- Schurr B, Asch G, Rietbrock A, Trumbull R, Haberland C (2003) Complex patterns of fluid and melt transport in the central Andean subduction zone revealed by attenuation tomography. *Earth Planet Sci Lett* 215:105–119
- Shapiro NM, Koulakov IY (2015) Probing the underbelly of a supervolcano. *Science* 348:758–759
- Smith WHF, Sandwell DT (1997) Global seafloor topography from satellite altimetry and ship depth soundings. *Science* 277:1957–1962
- Strack K-M (1992) Exploration with deep transient electromagnetics (Methods in Geochemistry and Geophysics). Elsevier Science Ltd, p 374
- Subandriyo, Purbawinata MA, Igushi M, Ishihara K, Young KD, Voight B (1997) Characteristics of tilt changes associated with Merapi during the 1993–1997 eruption. Abstracts—Merapi Decade Volcano international workshop II, Yogyakarta, Indonesia, p 18
- Surono JP, Pallister J, Boichu M, Buongiorno MF, Budisantoso A, Costa F, Andreastuti S, Prata F, Schneider D, Clarisse L, Humaida H, Sumarti S, Chr B, Griswold J, Carn S, Oppenheimer C, Lavigne F (2012) The 2010 explosive eruption of Java's Merapi volcano—a '100-year' event. *J Volcanol Geotherm Res* 241–242:121–135
- Syracuse EM, Abers GA (2006) Global compilation of variations in slab depth beneath arc volcanoes and implications. *Geochem Geophys Geosyst* 7(5): Q05017
- Telford WM, Geldart LP, Sheriff RE (1990) Applied Geophysics (2nd edn), Cambridge University Press, p 770
- Tiede C, Camacho AG, Gerstenecker C, Fernandez J, Suyanto I (2005) Modeling the density at Merapi volcano area, Indonesia, via the inverse gravimetric problem. *Geochem Geophys Geosyst* 6(9):Q09011
- Toutain J, Sortino F, Baubron J, Richon P, Surono SS, Nonell A (2009) Structure and CO₂ budget of Merapi volcano during inter-eruptive periods. *Bull Volcanol* 71:815–826
- Troll VR, Hilton DR, Jolis EM, Chadwick JP, Blythe LS, Deegan FM, Schwarzkopf LM, Zimmer M (2012) Crustal CO₂ liberation during the 2006 eruption and earthquake events at Merapi volcano Indonesia. *Geophys Res Lett* 39:L11302
- Troll VR, Deegan FM (2023) The magma plumbing system of Merapi: The petrological perspective. In: Gertisser R, Troll VR, Walter TR, Nandaka IGMA, Ratdomopurbo A (eds) Merapi volcano—geology, eruptive activity, and monitoring of a high-risk volcano. Springer, Berlin, Heidelberg, pp 233–263
- Vozoff K (1991) The magnetotelluric method. In: Nabighian MN (ed) Electromagnetic methods in

- applied geophysics, vol 22, pp 1943–1961. <https://doi.org/10.1190/1.9781560802686.ch8>
- Wagner D, Koulakov I, Rabbel W, Luehr B-G, Wittwer A, Kopp H, Bohm M, Asch G MERAMEx Scientists (2007a) Joint inversion of active and passive seismic data in Central Java. *Geophys J Int* 170(2):923–932
- Wagner D, Rabbel W, Luehr B-G, Wassermann J, Walter TR, Kopp H, Koulakov I, Wittwer A, Bohm M, Asch G, the MERAMEx Scientists (2007b) Seismic structure of Central Java. In: Karnawati D, Pramumijoyo S, Anderson R, Husein S (eds) *The Yogyakarta Earthquake of May 27, 2006*. Star Publishing Company, Belmont, California, pp 1–2
- Walter TR, Wang R, Luehr B-G, Wassermann J, Behr Y, Parolai S, Anggraini A, Günther E, Sobiesiak M, Grosser H, Wetzler H-U, Milkereit C, Brotopuspito KS, Harjadi P, Zschau J (2008) The 26 May 2006 magnitude 6.4 Yogyakarta earthquake south of Mt. Merapi volcano: did lahar deposits amplify ground shaking and thus lead to the disaster? *Geochem Geophys Geosyst* 9(5):Q05006
- Waltham D, Hall R, Smyth HR, Ebinger CJ (2008) Basin formation by volcanic-arc loading. *Geol. Soc Am Spec Paper* 436:11–26
- Wegler U (2003) Analysis of multiple scattering at Vesuvius volcano, Italy, using data of the TomoVes active seismic experiment. *J Volcanol Geotherm Res* 128(1–3):45–63
- Wegler U, Luehr B-G (2001a) Scattering behaviour at Merapi volcano (Java) revealed from an active seismic experiment. *Geophys J Int* 145:579–592
- Wegler U, Luehr B-G, Ratdomopurbo A (1999) A repeatable seismic source for tomography of volcanoes. *Ann Geofis* 42(3):565–571
- Wegler U, Luehr B-G (2001b) Multiple scattering of seismic signals at Merapi Volcano (Java, Indonesia)—results of an active seismic experiment (extended abstract). *Tohoku Geophys J (Sci Rep Tohoku Univ Ser 5)* 36:295–296
- Wegler U, Luehr BG, Zschau J, Maercklin N, Riedel C, Rabbel W (2000) Multiple seismic scattering effect at Mount Merapi - active seismic measurements help to explain complex earthquake signals of a strato volcano. *DGG-Mitt Spec Issue IV/2000*:43–48
- Westerhaus M, Rebscher D, Welle W, Brodscholl A, Pfaff A, Körner A, Nandaka GM (1998) Deformation measurements at the Flanks of Merapi Volcano. *DGG-Mitt Spec Issue III(1998)*:93–99
- Whitley S, Halama R, Gertisser R, Preece K, Deegan FM, Troll VR (2020) Magmatic and metasomatic effects of magma-carbonate interaction recorded in calc-silicate xenoliths from Merapi volcano (Indonesia). *J Petrol* 61(4):egaa048
- Widiyantoro S, Ramdhan M, Métaixian J-P, Cummins PR, Martel C, Erdmann S, Nugraha AD, Budi-Santoso A, Laurin A, Fahmi AA (2018) Seismic imaging and petrology explain highly explosive eruptions of Merapi Volcano, Indonesia. *Sci Rep* 8:13656
- Wilson P, Rais J, Reigber C, Reinhart E, Ambrosius BAC, Le Pichon X, Kasser M, Suharto P, Dato' Abdul Majid, Dato' Paduka Awang Haji Othman Bin Haji Yaakub, Almeda R, Boonphakdee C (1998) Study provides data on active plate tectonics in southeast Asia region. Wilson, Patricia et al. "Study provides data on active plate tectonics in southeast Asia region. *Eos* 79:545–549
- Wittwer A (2010) Investigating the crustal and upper mantle structure of the central Java subduction zone with marine wide-angle seismic and gravity data. Ph.D. Thesis, Christian-Albrechts-Universität, Kiel, Germany
- Wölbner I, Rumpker G (2016) Crustal thickness beneath Central and East Java (Indonesia) inferred from P receiver functions. *J Asian Earth Sci* 115:69–79
- Young KD, Voight B, Subandriyo S, Miswanto CTJ (2000) Ground Deformation at Merapi Volcano, Java, Indonesia: distance changes, June 1988–October 1995. *J Volcanol Geotherm Res* 100(1–4):233–259
- Yuan X, Ni J, Kind R, Mechie J, Sandvol E (1997) Lithospheric and upper mantle structure of southern Tibet from a seismological passive source experiment. *J Geophys Res* 102:27491–27500
- Zimmer M, Erzinger J, Sulistiyo Y (2000) Continuous chromatographic gas measurements on Merapi volcano, Indonesia. *DGG-Mitt Spec Issue IV/2000*:87–91
- Zschau J, Sukhyar R, Purbawinata MA, Luehr B-G, Westerhaus M (2003) The Merapi-project—interdisciplinary monitoring of a high-risk volcano as a basis for an early warning system. In: Zschau J, Küppers A (eds) *Early warning systems for natural disaster reduction*. Springer, Berlin, Heidelberg, pp 527–532